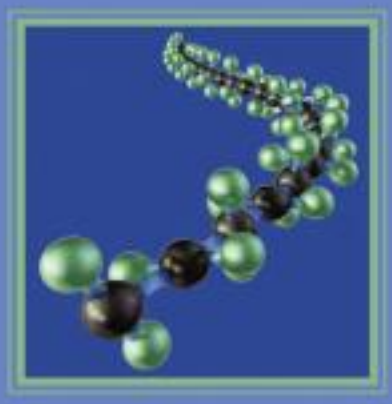

Encyclopedia *of* Polymer Science and Technology

FOURTH EDITION

Herman F. Mark

WILEY

POLYMER CHARACTERIZATION: ELECTRON PARAMAGNETIC RESONANCE

1. Introduction

Polymers and their nanocomposites are widely used in our daily life. The field of their use is permanently expanding. They are successfully used in pharmaceutics, medical therapy, aircraft and spaceship construction, and so on (1). One of the main scientific goals is to reinforce human brain with computer ability (2). To create such a symbiotic intelligence, appropriate neurochips were planned to be developed and created. However, a convenient modern computer technology is based on three-dimensional silicon crystals, whereas human organism consists of lower dimensional biological object. So, the combination of a future computer based on organic insulating and conjugated polymers with biopolymers is expected to considerably increase the power of human apprehension. The information in such elements can be transferred through conjugated polymers, for example, *trans*-polyacetylene (*trans*-PA), poly(*p*-phenylene) (PPP), polypyrrole (PP), polyaniline (PANI), polythiophene (PT), and their derivatives (3). Their electrical conductivity of either *p*- or *n*-type can be changed by more than 12 orders of magnitude by chemical or electrochemical introduction into their volume of various anions (BF_4^-, ClO_4^-, AsF_5^-, J_3^-, $FeCl_4^-$, MnO_4^-, and so on) or cations (Li^+, K^+, Na^+, and so on) or cations (Li^+, K^+, Na^+, and so on), respectively (4). The handling of charge transfer in such polymers becomes possible due to the existence in their backbone of alternating single and double bonds. This originates the appearance of midgap in their band structure as a result of the overlapping of π orbitals of monomer rings that depends on polymer structure, morphology, chain packing, and doping level y (the number of the dopant molecules per each polymer unit). Both the molecular and band structures of PT are shown in Figure 1 as an example. For this and analogous polymers, a resonance form can be derived, which corresponds to a quinoid structure. So, energetically lower and higher, benzenoid and quinoid forms can be stabilized in conjugated polymers under their chemical or electrochemical doping up to intermediate level y or irradiation (Fig. 1). As a result, the nonlinear excitations, polarons with spin $S = ½$ and elemental charge e, are formed on polymer chains. Their energy level lies in the midgap above the valence band (VB) and below the conducting band (CB) (Fig. 1). At the polymer doping up to intermediate level, polaron pairs may collapse and form spinless bipolarons (Fig. 1). The width of the polaron and bipolaron is 3–5 and 5–5.5 polymer units, respectively (5). With the further increase in a doping level y, bipolaron states overlap forming bipolaron

Encyclopedia of Polymer Science and Technology.
DOI: 10.1002/0471440264.pst511.pub2

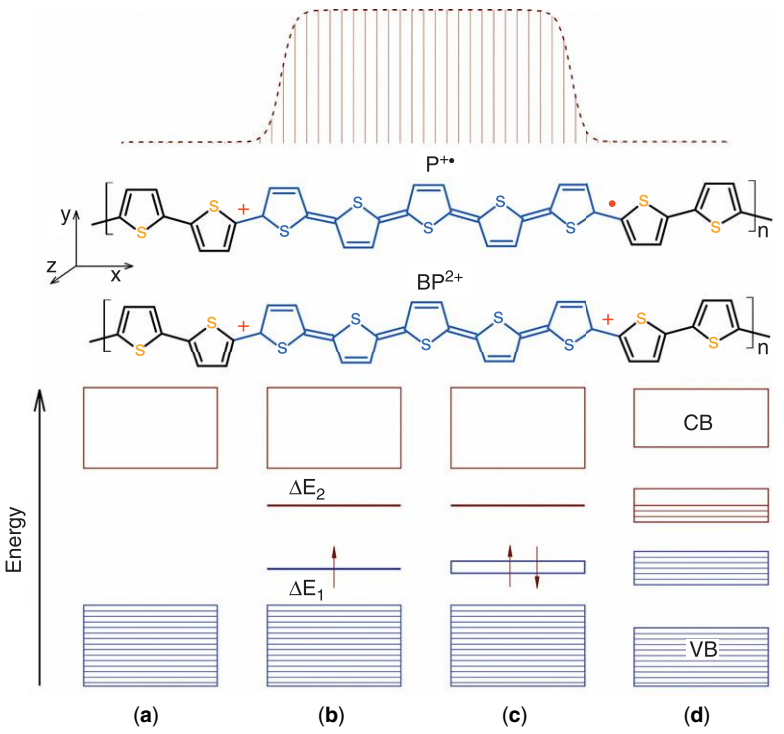

Fig. 1. Evolution of an initial band structure of polythiophene (**a**) under the polymer doping: (**b**) slight doping level with the appearance of polaron states in the bandgap, (**c**) intermediate doping level, with the appearance of states of noninteracting bipolarons, (**d**) high doping level, where bipolaron states overlap and form filled and semifilled bands with quasi-metallic behavior; the formation of a spin charged polaron $P^{+\bullet}$ and spinless bipolaron BP^{2+} on the polymer chain is shown. The distribution of the spin on the polaron is shown by dashed line.

bands within the gap. At a high doping level, these bands tend to overlap and create new energy bands that may merge with the VB and CB. Direct current (*dc*) conductivity of some soluble iodine-doped PT derivatives, poly(3-dodecylthiophene) (P3DDT) can reach 10^5 S/m (6). This accelerates quasi-three-dimensional (Q3D) charge transfer in such organic quasi-metals. The energy levels ΔE_1 and ΔE_2 of polarons depend on the polymer structure, morphology, and the nature of dopant molecule.

One of the fundamental peculiarities of the main conjugated polymers is that their units may rotate near own main axis. This stipulates the appearance of torsion (dihedral) angle θ between their planar units (7). Such an angle appears as a compromise between the effect of conjugation and crystal-packing energy, which would lead to a planar morphology, and the steric repulsing between ortho-hydrogen atoms, which would lead to a nonplanar conformation. This parameter reaches, for example, 23^o in PPP (8) and 56^o in leucoemeraldine base form of PANI (9). Its variation effects strongly charge transfer along conjugated polymer chains, whereas libration of polymer end groups modulates charge

transport between polymer chains. The effects of molecular disorder on electronic properties of the PT and analogous conjugated polymers can be accounted for by torsional disorder alone (10). An increase in ring torsion between two neighboring monomers can cause electron localization and then change the charge transport from adiabatic polaron drift to nonadiabatic polaron hopping.

Various methods, for example, conductometric, viscosimetric, and optical (fluorescence and phosphorescence), can be used for the study of paramagnetic centers (PC) stabilized or/and initiated in polymers and their nanocomposites (11). The spin nature of atoms and quasi-particles forming in a polymer network stipulates the use of complimentary nuclear magnetic resonance (NMR) and electron paramagnetic/spin resonance (EPR/ESR) methods for accurate elucidation of the structure, dynamics, and function of various macromolecular and supramolecular systems (12). EPR spectroscopy discovered by Soviet physicist Eevgeny Zavoisky at the Kazan State University in 1944 (13) was proved (14) to be well-established, widely used, and productive physical direct method in studies of ion radicals, molecules in triplet states, transition metal complexes, high-molecular systems with stabilized or initiated PC. This method is used for the study of various inherent polymers characteristic phenomena including the structural defects and degradation, charge transfer and redox activity, paraelectric–ferroelectric transitions, catalytic activity, adsorption and desorption behavior, host–guest interactions, magnetic exchange pathways, postsynthetic modifications or functionalization, and so on (15). It is based on resonant absorption of microwave (MW) radiation by unpaired electrons due to the splitting of their energy levels in an external magnetic field. Unpaired electrons of each spin systems characterizing by the Landé splitting factor g. If the fundamental resonance condition

$$\hbar\omega_e = \gamma_e \hbar B_0 = g\mu_B B_0 \tag{1}$$

is fulfilled (here $\hbar = h/2\pi$ is the Planck constant, $\omega_e = 2\pi\nu_e$ is the angular electron precession frequency, γ_e is the hyromagnetic ratio for electron, B_0 is the magnitude of external magnetic field, and μ_B is the Bohr magneton); an unpaired electron absorbs an energy quantum and is transferred from ground state to a higher excited state. This is accompanied by a change in the direction of the spin to the opposite as illustrated in Figure 2.

Free electron occupying an atomic s-orbital is characterized by single EPR line and the Landé factor $g_e = 2.002319$. In real solids, the configuration of a cloud of spin density is more complex, so that this parameter becomes a tensor with the main terms (16):

$$g_{ii} = g_e \left(1 + \frac{\lambda\rho(0)}{\Delta E_i}\right) \tag{2}$$

where λ is the spin–orbit coupling constant, $\rho(0)$ is the spin density, $\Delta E_i = \Delta E_{n\pi^*}$ and $\Delta E_{\sigma\pi^*}$ are the energies of spin resonant transition $n \rightarrow \pi^*$ and $\sigma \rightarrow \pi^*$ at respective orientation of its molecular x and y axes in the external magnetic field, respectively (Fig. 1). At the z-orientation, the respective term of the g factor lies near g_e. This provokes its difference from g_e at reorientation of PC in an external magnetic field. An effective (isotropic) g factor of PC with, for example,

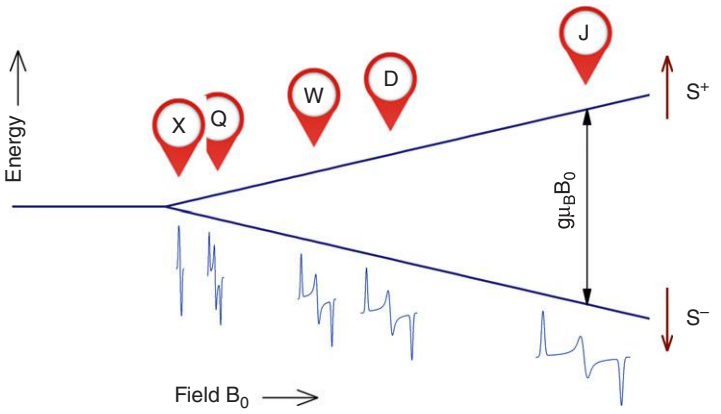

Fig. 2. Splitting of the ground state of the spin at different values of the external magnetic field B_0. EPR spectra of PC with $S = ½$, $g_{xx} = 2.00598$, $g_{yy} = 2.00211$, and $g_{zz} = 1.99860$ calculated for respective spin precession frequencies are shown.

rhombically distributed spin density consists of three main terms, $g_{\text{iso}} = {}^{1/3}(g_{xx} + g_{yy} + g_{zz})$.

For long time, EPR investigations are predominantly carried out at convenient 3-cm or X band with $\nu_e \leq 10$ GHz and $B_0 \leq 330$ mT. At these wavebands, however, the signals of organic free radicals with the g factor lying near g_e are registered in a narrow magnetic field range and, therefore, can overlap the lines with close g factors. Besides, strong cross-relaxation of PC still perceptible at low magnetic fields (17) additionally complicates the registration and identification of such centers. This is why PCs in organic systems demonstrate low-informative single spectra that allow to measure directly only their line shape and concentration. The new experimental techniques improving the efficiency of EPR spectroscopy in the study of solid-state systems were developed. They are electron spin echo spectroscopy (11a, 18), method based on the effect of spin polarization, in which EPR signal is registered optically (19), methods of double electron-nuclear resonance (20), spin label and probe method (21), MW saturation transfer EPR (ST-EPR) method (22), and so on. However, the most of these methods may be applied only to solve specific problems and investigate special objects.

Earlier, it was demonstrated (23) that the efficiency of the method can be increased sufficiently at millimeter wavebands EPR. At D-band EPR, it was investigated in detail structure, relaxation, dynamics, and other specific characteristics of radical centers and their local environment, and elementary charge transfer processes in different solids, including biopolymers and organic polymers. Some polyacetylene films were investigated at 9.7–430 GHz wavebands EPR (24). Figure 2 shows exemplary EPR spectra of PC with $S = ½, g_{xx} = 2.00598$, $g_{yy} = 2.00211$, and $g_{zz} = 1.99860$ calculated for various spin precession frequencies. It is seen that they consist of three components registered at different values of B_0 (see Fig. 2). The splitting between individual spectral components increases with ν_e (and, therefore, with B_0). So, to identify all the main resonant terms of PC with anisotropic parameters for their further analysis, both the ν_e and B_0 values

Table 1. EPR bands, MW frequency and magnetic field strength necessary for resonant transition of free electrons with $S = ½$ and $g_e = 2.002324$

Bands	*L*	*S*	*C*	*X*	*P*	*K*	*Q*	*U*	*V*	*E*	*W*	*F*	*D*	–	*J*	–
F, GHz	1	3	4	10	15	24	35	50	65	75	95	111	140	190	285	360
B_0, T	0.03	0.11	0.14	0.33	0.54	0.86	1.25	1.8	2.3	2.7	3.5	3.9	4.9	6.8	10.2	12.8

should be optimally increased. EPR bands with appropriate ν_e and B_0 values are summarized in Table 1. The choice of the optimal EPR band depends on the research goals, experimental conditions (temperature, irradiation, and so on) and the properties of the sample. It allows getting detailed information on its structural properties as well as molecular and electronics processes carried out in its bulk.

Measurements at millimeter EPR wavebands (14d, 21b, 23c–e,g,h, 25) offer the following advantages of the method:

1. EPR spectra are simplified due to the reduction of second-order effects at high fields;
2. increase in orientation selectivity and sensitivity in the investigation of disordered systems;
3. the informativity and precision of pulse methods, for example, electron nuclear double resonance (ENDOR) also increase at high magnetic fields;
4. accessibility of spin systems with larger zero-field splitting due to the larger MW quantum energy $h\nu_e$;
5. higher spectral resolution over the *g* factor, which increases with the spin precession frequency ω_e and external magnetic field B_0. This is used to investigate the structure, polarity, and dynamics of radical microenvironments in spin-modified organic and biological systems by the spin label and probe method;
6. saturation of PC occurs at a comparatively low MW magnetic term B_1, due to the exponential dependence of the number of excited spins on the radiation frequency ν_e. This effect can be successfully used to study the relaxation and dynamics of PCs as well as of superslow motion in the systems under study;
7. cross-relaxation of PCs decreases dramatically at high magnetic fields, making it easier to obtain more precise and more complete information about the system under study.

It should, however, be noted that the advantages of the high-frequency/field EPR spectroscopy are limited in practice by a concentration sensitivity that decreases with increasing MW frequency. Indeed, as EPR spectrum of PC with anisotropic magnetic parameters is more stretched across the field at higher ν_e, its intensity follows the $\nu_e^{-0.87}$ power function. Nevertheless, high-frequency/field EPR spectroscopy allowed to obtain qualitative new information on various condensed systems and to solve various scientific problems.

We describe the results of the study of exemplary insulating, biological, and conjugated polymers obtained at 9.7–140 GHz wavebands CW EPR mainly

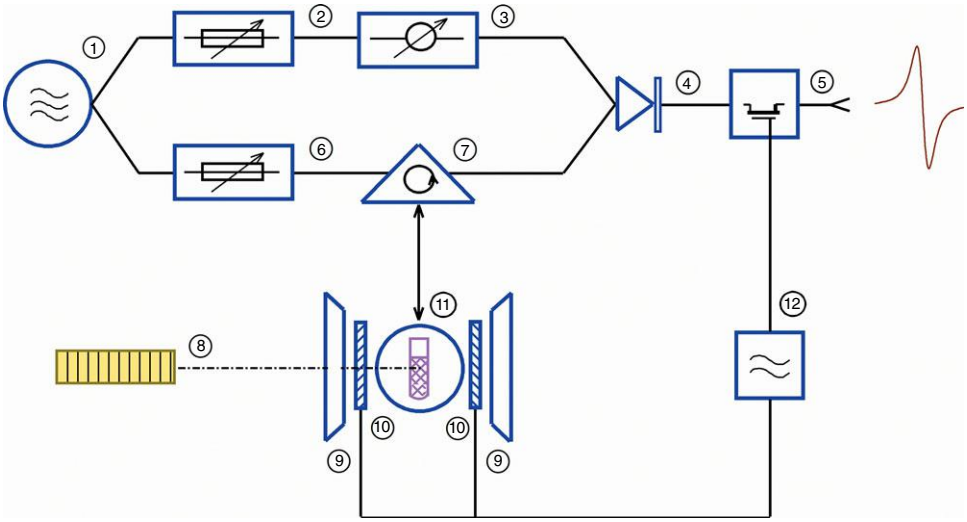

Fig. 3. The sketch of X-band EPR spectrometer: ***1***, MW oscillator; ***2***, MW attenuator; ***3***, MW phase shifter; ***4***, MW detector; ***5***, *ac* phase detector; ***6***, MW attenuator; ***7***, MW circulator; ***8***, light source (laser); ***9***, magnet poles; ***10***, *ac* modulation coils; ***11***, MW cavity with a sample; ***12***, *ac* oscillator.

carried out at The Institute of Problems of Chemical Physics, Russian Federation. The use of the EPR method to study other polymer systems is well described in the literature (14c,d,i, 15), and (26). It is organized as follows: The next section describes experimental setup, EPR technique, and standards used at the study of polymer systems with domestic and initiated PC. The results of the study of PC stabilized in exemplary insulating, biological, and conjugated polymers obtained by using of multifrequency EPR spectroscopy combined with the steady-state saturation of spin packets, spin label, spin probe, and saturation transfer methods are discussed in the third, fourth and fifth sections, respectively.

2. Instrumentation and Experimental Setup

2.1. EPR Techniques. When studying polymer systems, the EPR technique and waveband are chosen according to the details of the set goal. The spectrometers used at all wavebands are designed according to the uniform scheme (14d). The simplest, 3-cm waveband EPR spectrometer most frequently used in the study of various condensed media is shown schematically in Figure 3. The main parts of this device are MW power oscillator *1*, magnet ***9*** and MW cavity/resonator ***11***. MW power is generated by oscillator ***1*** based on klystron or solid-state klystron or Gunn diode. It is split and transmitted to the two branches of the MW bridge. The referent part of the bridge consists of MW attenuator ***2*** and MW phase shifter ***3***, whereas the signal measuring part contains more precession MW attenuator ***6***, one-way MW circulator ***7***, and MW cavity ***11*** situated between the magnet poles ***9***. The sample under study in quartz ampoule is placed at the center of the MW cavity ***11*** and both the branches are tuned to reach balanced zero

signal at the output of the MW diode ***4***. Once the relation equation (1) fulfilled for PC analyzed, they are excited to the higher energy level absorbing a little part of MW energy in a measuring branch. This causes imbalance in the MW bridge and appearance at its output of resonant *ac* signal under a scanning of external magnetic field B_0 by additional *ac* coils ***10***. This signal is transformed into final *dc* EPR response by a phase detector ***5***. Normally, the cavity and magnet of the spectrometer are provided with a through hole through which the PC in the sample can be initiated under direct irradiation or illumination by appropriated source ***8***. The more spins are stabilized or/and initiated in the sample the higher integral signal is registered. A typical EPR spectrometer is characterized by a sensitivity of 4×10^{11} spins per mT, resonance instability of 3×10^{-5} per hour, maximal MW power 150 mW inducing $B_1 = 48\ \mu$T in the center of the cavity with the MW mode H_{102} and a unloaded quality factor $Q_0 \approx 5000$.

The minimal number of registered spins $N_{\min}$, that is the sensitivity of the EPR method, depends on the spin precession frequency ω_e,

$$N_{\min} = \frac{k_1 V}{Q_0 k_f P^{1/2} \omega_e^2} \tag{3}$$

where k_1 is constant, V is sample volume, k_f is filling coefficient, P is MW power applied to a cavity input. With k_f and P being constants $N_{\min} \propto (Q_0 \omega_e^2)^{-1}$ and $Q_0 \propto \omega_e^{-1/2}$, that is $N_{\min} \propto \omega_e^{-\alpha}$, where $\alpha = 1.5$ (27). In practice, α can be varied from 0.5 to 4.5 (27) depending on spectrometer modification, registration conditions, and a sample size.

If some PC with near magnetic parameters appear in a sample, their lines can overlap. The width of individual EPR lines of most organic radicals usually amounts to 0.1–1.0 mT, and a g-factor value differs from g_e by $(1–10) \times 10^{-4}$. Therefore, the spectral resolution or splitting of lines of different radicals, $\delta B \cong \delta g B_0 / g \cong 10–100$ mT is less than their width at a 3-cm waveband, resulting in the overlapping of their EPR spectra. This complicates the identification of such radials in solids by using their g factors and the analysis of structural and dynamic properties of their microenvironment (14d). This means that to attain the satisfactory resolution of free radicals' EPR spectra, the condition $\delta B / B_0 < 2 \times 10^{-5}$ should be valid. If the linewidth of PC does not change with registration frequency, such a condition is fulfilled at millimeter wavebands EPR. Besides, the susceptibility of the method also increases at high spin precession frequency ω_e (23e,h, 25k). According to equation (1), the registration of PC with $g \cong 2$, for example, at the D-band (140 GHz, 2-mm) EPR requires MW power source and a strong (near 5 T) permanent magnetic field. Conventional metals may induce magnet field up to ~1.2 T, so cryogenic systems based on a superconducting solenoids are the most promising for inducing of so strong magnetic fields. Currently, superconducting magnets, providing magnetic fields with the intensity up to 30 T and the inhomogeneity up to 10^{-15} m^{-3}, are commercially available and widely used in magnetic spectroscopy. The Bruker Corporation has developed and started supplying in scientific centers of continuous wave (CW) and pulse EPR spectrometers operating at wide (1–263 GHz) wavebands. The devices of a submillimeter range with a laser source of polarizing radiation have magnet-producing field strength up to 100 T

in a pulse regime inside a multisectional superconducting solenoid of a peculiar shape (28). However, the field of application of this device is strongly restricted because of its low concentration sensitivity, stipulated by a unit quality value of a measuring cavity, and a high cost of its cryogenic equipment. The home-made EPR spectrometers operating at the spin precession frequency from a few MHz (29) up to a few THz (30) corresponding to 10^2–10^{-6} m wave lengths also used in the study of various objects. This makes it possible to study even living small animals at the low-frequency/field EPR bands, as well as point-like samples in millimeter ones.

2.2. EPR Standards. A quite important problem is to choose the appropriate standards for a precise device tuning, a magnetic field scanning, and *g*-factor scale calibration. The standard must be arranged close to a sample inside a small cavity; therefore, it must produce a sufficiently intensive narrow signal, being of a small size. Various compounds may be used as *g* standards in EPR spectroscopy.

Paramagnetic ions Mn^{2+} diluted in diamagnetic matrices are widely used as EPR standards (31). For example, Mn^{2+} traces in MgO with nuclear spin $I = 5/2$, isotropic hyperfine interaction constant $a = 8.74$ mT and effective $g_{\text{eff}} = 2.00102$ is frequently utilized as most simple standard in EPR experiments for calibration of *g*-factor and an external magnetic field. At centimeter wavebands, it can be used as lateral standard situated near a sample under study. However, the second-order correction to its effective resonance field, $\delta B = a^2[(I(I + 1) - m^2]/2B_0$ (here m is the orientation magnetic number) (32), should be taken into account. This value at, for example, 3-cm waveband can reach 65 μT. At millimeter wavebands, this correction does not contribute to an essential error to the magnetic parameters measurement and can be neglected. So, it can be used as a standard suitable for the *g*-factor scaling at high-field EPR experiments (23c,d) and remains the favorite standard in many labs using the millimeter waveband EPR technique. At high-field wavebands, the ubiquitous six line spectrum has very sharp lines due to the reduction of second-order effects and effectively provides a field calibration over a 40-mT range (five distances between lines split by 8.7 mT as a hyperfine interaction constant). It can be either attached by a toluene solution of polystyrene to one of the MW cavity plungers (23c,d) or used as environmental quasi-matrix of a powder-like sample under study (33). The signal intensity of this standard is conveniently regulated by plunger rotation about its axis, that is due to the change in the angle between the B_0 and B_1 directions in the place of its position.

Single crystal 2,2-diphenyl-1-picrylhydrazyl (DPPH) possessing a spin $S = ½$ in each molecule seems to be the other well-known standard due to its extremely intense line. However, its use at high fields has been hampered (34) by the fact that the *g*-factor depends on the solvent used under DPPH preparation by its recrystallization and, even then different crystal quality under the same preparation are sometimes found to have *g*-factors varying within 2.0030–2.0043 range.

Some organic ion-radical single crystals can also be used for calibration of *g*-factors (35). One of them, $(\text{fluoranthene})_2PF_6$, has extremely narrow peak-to-peak linewidth ($\Delta B_{\text{pp}} \leq 5$ μT at 95–140 GHz) and the value of its *g*-factor is known to a high degree of accuracy, $g_{xx} = 2.00226$, $g_{yy} = 2.00258$, $g_{zz} = 2.00222$ (needle axis). The single crystals of $(\text{naphthalene})_2PF_6$ and $(\text{perylene})_2PF_6$ demonstrate solitary EPR spectra with $\Delta B_{\text{pp}} = 0.18$ mT, $g = 2.00316$, and $\Delta B_{\text{pp}} = 0.15$ mT,

$g = 2.00321$, respectively. This allows them to be easily recognized and differentiated by adjusting the magnitude of the modulating field in the study of most organic solids. Besides, it can be used for determination of relaxation parameters using the CW saturation method. Note, however, that it cannot be used at temperatures much below 200 K due to a phase transition. If one keeps the sample at high temperature and air presence, it is also slowly deteriorates over time. More stable single crystals of (dibenzotetrathiafulvalene)$_3$PtBr$_6$ ((DBTTF)$_3$PtBr$_6$) are characterized by strong EPR line with $\Delta B_{pp} = 0.44$ mT and $g = 2.01628$. The precise device adjustment in the registration of a real χ' or an imaginary χ" components of paramagnetic susceptibility is obtained by an attainment of the symmetric first and second derivatives of dispersion and absorption standard signals, respectively, in the device output. The phase of *ac* modulation frequency ω_m is most finely adjusted by a minimum $\pi/2$-out-of-phase unsaturated signal of a standard with the following phase change by $\pi/2$ (36). In this case, the $\pi/2$-out-of-phase signal attenuation is not less than 23 dB. It was shown (35) that this single crystal being placed in a condensed system can be reoriented in high magnetic field, so its line is shifted by around 28 mT in ~5 T magnetic field. This effect may be successfully used for the study of physical properties of some viscous media (see below).

Isolated paramagnetic vacancy V_{Si}^- in 3C-SiC that exhibits a narrow, near 50 μT, strong and stable resonance EPR signal observable within 1.2–300 K temperature region and does not show any aging effect (37) can also be used in some experiments.

A KC_{60} metallic fullerene crystalline polymer has the advantage of a temperature independent intensity, linewidth near 0.2 mT and resonance position within a wide temperature region (38). It was stated that this material is a suitable standard for a large temperature range (from 3 to 300 K) and frequency (tested up to 225 GHz) range. It has temperature independent magnetic spin susceptibility and only small variations in the linewidth with temperature and frequency. The material is inert; it does not degrade under atmospheric conditions. It has a large magnetic susceptibility and can thus be used in low sensitivity apparatus. The spin–lattice relaxation rate is fast at low temperatures thus saturation problems are not important in the CW EPR study of solid-state samples, especially organic and classic metals. Its usefulness by measuring the susceptibility of a newly synthesized two-dimensional fulleride polymer, $Mg_{4+x}C60$, was demonstrated. Another fullerene-based material, P@C_{60} or N@C_{60} (C_{60} fullerene molecule with encapsulated ^{31}P or ^{14}N atom) embedded in C_{60} crystalline matrix, is characterized by extremely narrow (less than 10 μT) linewidth (39) and may be used as a *g*-factor standard as well. It demonstrates a characteristic ^{31}P doublet (with isotropic hyperfine interaction constant $a_{iso} = 4.94$ mT) or ^{14}N triplet (with $a_{iso} = 0.5665$ mT) spectrum with no additional fine structure splitting at ambient temperatures due to fast rotation of the molecule. At lower temperatures, a rotation is frozen and a spin–lattice relaxation becomes longer but fine structure splitting remains small. It is not sensitive to exposure in air.

Li:LiF characterized by a narrow (less than 0.1 mT) solitary EPR spectrum with $g = 2.002293$ (40) may also be used as high-frequency/field EPR standard for *g*-calibrations within, for example, a field range of about 28 mT for the Bruker E680 94 GHz spectrometer, which is well sufficient for typical organic radicals.

There is very good reproducibility of the field measurements on repetitive removal of the Li:LiF sample and reinsertion into the probe head with a typical deviation of the line position in the range of 10 μT. This allows the use of this standard for calibration before and after the measurement of interest as long as the reproducibility of the field sweep is sufficient. Major disadvantage is line shape distortions depending on sample quality.

Some organic conducting polymers, for example, PANI, are characterized by high concentration of stable spins. They are mainly insensitive to the environment, cheap, widespread, and may also be used as an EPR standard.

1,3-*bis*-Diphenylene-2-phenyl-allyl being embedded into polymer matrix are characterized by high spin concentration and, therefore, fast spin relaxation (41). However, it is characterized relatively broad (near 1 mT) EPR spectrum, which may interfere with $g = 2$ spectra. This makes such a system a suitable standard in an EPR study at relatively low temperatures.

2.3. Method of Spin Microprobe and Macroprobe. The abovementioned method of spin label and probe takes information about structure and dynamics of microenvironment of stable radical introduced into polymer matrix. Polymers, however, are characterized by strongly anisotropic structural and morphological parameters. If one modifies them with a nonspherical probe, then its effective rotation frequency should be defined by a complex dynamics of a radical and its microenvironment. Stable nitroxide radicals being inserted into the polymer system can be used not only as a spin probe (42) but also as a counterion (42c,43) in the study of organic conjugated polymers. The EPR spectrum of a polymer system modified by a nonspherical radical should depend on anisotropy of its magnetic resonance parameters and inhomogeneous microenvironment. The relaxation changes in the EPR spectrum of a randomly oriented spin-modified system should not appear for that fraction of radicals which are mainly oriented with the preferred rotation axis along the field. This means that for a radical rotation near, for example, the molecular x-axis, relaxation changes should be manifested mainly in the spectral y and z components. Further acceleration of such a motion involves all spectral components accompanied by their broadening and shift to the center of the EPR spectrum. The broadening of these components, δB_i, is proportional to the frequency of slow ($v < 5 \times 10^8$ s^{-1}) radical reorientation with respect to the direction of the external magnetic field B_0 (23b-d,44):

$$\delta B_{\mathrm{x}} \approx 2\gamma_{\mathrm{e}}^{-1}\nu_{\perp} \tag{4}$$

$$\delta B_y = \delta B_z \approx \gamma_{\mathrm{e}}^{-1}(\nu_{\perp} + \nu_{||}) \tag{5}$$

where $\nu_{\perp}$ and $\nu_{||}$ are the rotation frequency of the radicals oriented perpendicularly and parallel to the direction of the external field., respectively. These conclusions are also valid for radicals with other main axes of preferred radical rotation.

It implies that at fast interactions of a spin probe with own microenvironment, the latter can be considered as an elastic medium. The correlation time τ_{c} of the radical motion should therefore be significantly smaller than that of mechanical relaxation of such an interaction and does not appear as a sufficiently informative parameter, characteristic of a dynamic process. The correct

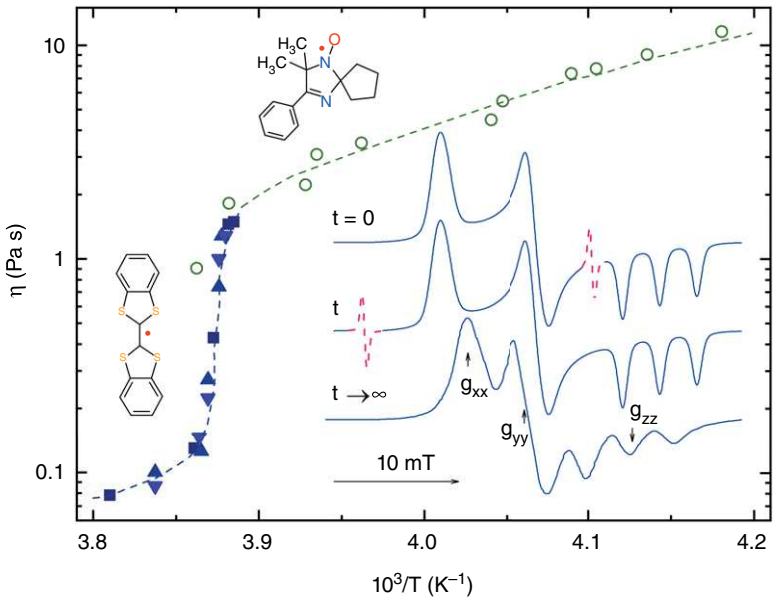

Fig. 4. The Arrhenius dependency of dynamic viscosity η of the nujol/*tert*-butylbenzene mixture (1:10) obtained by using of the nitroxide radical as spin microprobe (open symbols) and by using of single crystal (dibenzotetrathiafulvalene)$_3$PtBr$_6$ as a spin macroprobe (filled symbols, three single crystals with different sizes). In the insert are shown D-band EPR spectra of these spin probes introduced into frozen and heat softened mixture at $t = 0$ (upper spectrum), t at $T \leq T_g$ (middle spectrum), and $t \rightarrow \infty$ at $T \leq T_g$ (lower spectrum) time period.

interpretation of the results, obtained by using the spin probe method therefore implies the preliminary knowledge of structural and other properties of the system under study.

Krinichnyi and others showed (35) that for such an investigation can additionally be used for the so-called method of spin macroprobe, in which a comparatively massive paramagnetic with the characteristic sizes of about 10–100 μm is used as a probe. The method is based on the analysis of simultaneous rotation in the system under study of both the nitroxide radical and a single microcrystal of a suitable ion-radical salt placed into strong magnetic field. It was detected that, (DBTTF)$_3$PtBr$_6$ is oriented by own main crystal axis when the total dipole moment of its PC tends to be oriented along the direction B_0 to attain the minimum energy of spin interaction with the magnetic field. Such a reorientation process is easily registered by its EPR line shift into lower magnetic fields. The time of crystal orientation is a function of many parameters, such as its weight, size, effective magnetic momentum as well as medium viscosity, and the strength of external magnetic field applied.

In the insert of Figure 4, D-band EPR spectra of frozen nujol/*tert*-butylbenzene mixture (1:10) are shown in which an appropriate nitroxide radical is solved and (DBTTF)$_3$PtBr$_6$ single microcrystal is introduced into the mixture bulk as a spin microprobe and macroprobe, respectively. First, at the

temperature significantly exceeding the temperature T_g of the matrix glass transition, the latter is oriented to its main crystallographic axis along the magnetic field B_0. Then, a double spin-modified system is cooled down to $T \leq T_g$, turned by 90° (top spectrum in Fig. 4) and then it should be slowly warmed up to $T \cong T_g$. Once the matrix becomes softer, the EPR line of the spin macroprobe begins to move along the spectrum as shown on the middle spectrum in Figure 4. The line shift follows an exponential law and attains the maximal value, $\delta B \cong 20$ mT for this sample at $t \to \infty$ and $B_0 \approx 5$ T. This process is accompanied by a narrowing of spectral components of the nitroxide radical and their shift to its spectral center (bottom spectrum in Fig. 4).

Correlation time of the spin microprobe was determined from equation (4) in frames of Brownian diffusion rotation (21b) to follow activation law

$$\tau_c = \tau_c^0 \exp\left(\frac{E_a}{k_B T}\right) \tag{6}$$

with $\tau_c^0 = 4.7 \times 10^{-20}$ s and $E_a = 0.57$ eV (here k_B is the Boltzmann constant). The preexponential factor obtained exceeds considerably the inverted frequencies of molecular orientation oscillations in the condensed phase. Besides, the activation energy of radical rotation is higher than that typical for a pure solvent. This can be a result of correlation of the radical mobility and a segmental mobility of nujol extended molecules $(—CH_2—CH_2—)_n$, where $n > 10$.

The value characteristic of the orientation process of spin macroprobe is the time-dependent angle φ between its molecular axis and direction of the external magnetic field B_0 (35)

$$\varphi(t) = \varphi_0 \exp(-t/\tau_m) \tag{7}$$

where $\tau_m = 6\pi\eta b^3/(NV\mu_O\mu_B B_0)$ is the mechanical relaxation time for such reorientational process, η is the coefficient of dynamic viscosity of the matrix, b, N, and V are the characteristic size, volume, and bulk spin concentration of the microcrystal, respectively, μ_0 is the permeability for vacuum, and μ_B is the Bohr magneton. Then dynamic viscosity of the system can be determined from the Stokes equation:

$$\tau_c = 4\pi\eta r^3/(3k_B T) \tag{8}$$

where r is the hydrodynamic radius of spin microprobe (distance between N and O atoms in the nitroxide radical r_{NO}) or macroprobe (a characteristic size of microcrystal b).

Figure 4 depicts the temperature dependency of the viscosity of the model system, determined by both the complementary spin microprobe and spin macroprobe methods. It should be noted that the hydrodynamic radius of the nitroxide radical depends on the structure of the environment molecules and therefore varies in a wide range. By combining $\eta(T)$ dependencies, obtained by both methods, one obtains $r_{NO} = 0.14$ nm for the used nitroxide radical.

Extrapolating $\eta(T)$ dependency obtained by the method of spin microprobe, to higher temperature, one obtains $\eta = 0.11$ Pa s at $T = 300$ K, that is it falls

within a range of viscosity for different oils. However, such an extrapolation yields $\eta = 5.6 \times 10^{-3}$ Pa s at $T = 300$ K, by considering η jump at T_g. This confirms once more the correctness of the joint application of the complementary methods described as investigating relaxation and dynamic processes in various condensed systems. The method of spin macroprobe successfully enriches the method of spin probe and enables the possibility of a more accurate determination of dynamic viscosity in a wider temperature range. It becomes possible to characterize the mechanical losses in solutions of conjugated polymers, other condensed media in a stationary regime, and to establish their glass transition point in the case of extremal mechanical losses in these systems.

The dependency $\tau_m \propto b^3 B_0^{-1}$ is derived from equation (7). Considering the higher concentration and absolute sensitivities of the D-band EPR spectroscopy, one can draw a conclusion that the application of the method at this waveband widens the range of dynamic viscosity (and likely the other parameters as well) measurement in condensed systems by at least two orders of magnitudes as compared with other bands and a higher magnetic field strength.

3. Insulating Polymers

The most widely synthesized polymers, polystyrene, polyvinylchloride, nylon, and so on, are normally diamagnetic insulators. This means that to investigate such systems by the EPR method some number of molecules with unpaired electrons should be introduced into their bulk. This can be PC reversibly or irreversibly formed in a polymer bulk due to its irradiation by photons or introduced into a polymer as a spin label or spin probe during chemical or electrochemical synthesis. Because magnetic resonance parameters of such domestic and guest centers sense the properties of own microenvironment, by analyzing the changes in these parameters it became possible to investigate the structural, morphological, electronic, other properties of a polymer system. It is briefly considered below with some exemplary polymer systems.

3.1. Poly(1,1,2,2-tetrafluoroethylene). The advantages of the D-band EPR was clearly illustrated in the study of widely used poly(1,1,2,2-tetrafluoroethylene) (PTFE) (23b,45). PTFE samples were irradiated at $T = 77$ K by ^{60}Co source, dose 1 MGy, and then exposed to air. In results of such a procedure, the middle-type peroxide radicals are mainly formed in the initial PTFE sample with arbitrary oriented macromolecules. To obtain the end-type radicals, the specimens were irradiated in a vacuum with subsequent exposure to the air. Room temperature D-band EPR spectrum of the so-called sample is shown at the top of Figure 5 as superimposing on the single line of the end-type peroxide radical and the spectrum of the middle-type radical with the axial symmetry $\boldsymbol{g}$-tensor with $g_{\perp}^{\text{mid}} = 2.02100$ and $g_{||}^{\text{mid}} = 2.00560$.

The figure also shows the low-temperature spectra of PTFE samples, partially oriented by stretching. It can be seen that the intensity of the spectral y-component decreases drastically when the direction of magnetic field and sample stretching matches. This indicates that the corresponding molecular axis lies near the plane perpendicular to the stretching axis. The angle between the axis

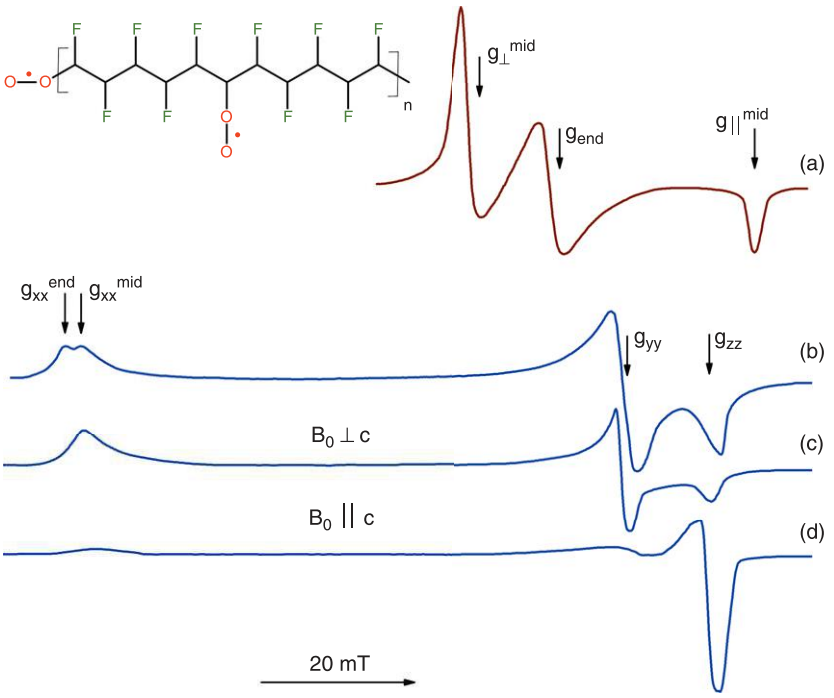

Fig. 5. D-band EPR spectra of the initial PTFE with chaotically oriented chains (**a**,**b**) as well as with the chains, partially oriented perpendicularly (**c**) and parallel (**d**) to the external magnetic field and registered at T = 300 K (**a**) and 100 K (**b**–**d**).

of the polymer lying in molecular xy-plane and the direction of the O–O bond was determined from the data obtained at this waveband to be 72°. The main values of $\boldsymbol{g}$-tensor middle- and end-type radicals were also determined: g_{xx} = 2.03818, g_{yy} = 2.00743, g_{zz} = 2.00232, and g_{xx} = 2.03963, g_{yy} = 2.00770, and g_{zz} = 2.00278, respectively.

3.2. Polyvinyl Chloride. A highly sensitive and selective sensor for water molecules based on another well-known polymer, polyvinyl chloride (PVC), was constructed and studied by both the EPR and conductometry methods (46). The initial polymer does not have neither free nor unpaired electrons. However, it was found that the treatment of PVC by fuming sulfuric acid leads to its appearance in matrix dingy regions (46). Such a modified material exhibited at room temperature a Lorentzian weak EPR singlet with ΔB_{pp} = 0.54 mT and g = 2.0031, characteristic of π-electron systems (Fig. 6). The linewidth and signal intensity changed weakly while the temperature decreased to T = 77 K. Magnetic parameters of this material appeared to be close to those of high-conductive domains formed in polyacetylene after its cis-trans-isomerization (47). Thus, the change in electronic and paramagnetic properties of the film can be explained by dehydrochlorination during its oleum treatment with the formation of *trans*-PA regions with unpaired electrons in neutral quasi-particles, $[—CHC1—CH_2—]_m \rightarrow [—CHCl—CH_2—]_m—[CH=CH\dot{=}CH=CH—]_n$ (Fig. 5). It was found that such prepared materials become a highly sensitive and selective

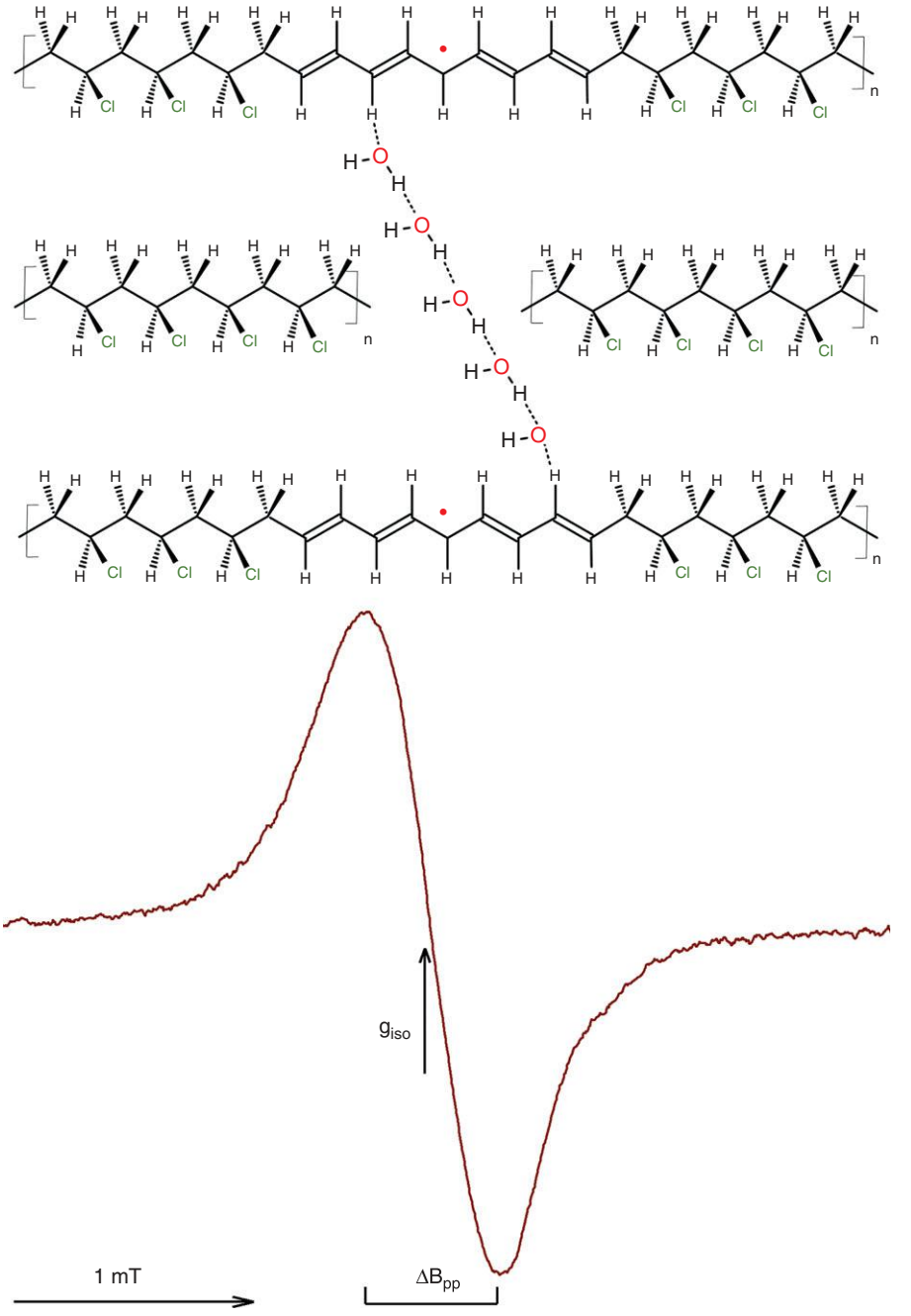

Fig. 6. The room temperature X-band EPR spectrum of the PVC treated by fuming sulfuric acid. The formation of *trans*-polyacetylene domains and interdomain Q1D water chain are shown schematically.

polymer sensor for water molecules. Such an effect can be explained in the following manner: Being weak electron acceptors, water molecules accept partially the electron density from such the solitary charge carriers (47), on the surface or on the bulk of the film, thus providing *p*-type conductivity of the domains. When the water molecules diffuse into the polymer bulk, they can form bridge-type hydrogen bonds between the conjugated chains (Fig. 6). As a result, the above-mentioned quasi-particles acquire a positive charge in the *trans*-PA domains. Moreover, in a modified PVC the so-called Davydov solitons (48) may also be formed in the quasi-one-dimensional (Q1D) spreading hydrogen bonded water associates, as in other low-dimensional nanosystems (49). Such nonlinear quasi-particles can also transfer charges between *trans*-PA chains. Thus, the macroconductivity of the sample contacting water vapor increases considerably as a result of both intra- and interchain charge transfer. Other molecules are not able to form such associations that determine the selectivity of the sensor to water molecules only. Such a feature can be used in highly efficient molecular sensors.

4. Biological Polymers

4.1. Cotton Fibers and Cellulose. Natural polymer fibers, including cellulose and cotton, which consists of 92–98% cellulose, are found to be promising as matrices for artificial catalysts, modeling biological enzymes (1a). Catalytic properties of such biocatalysts are defined mainly by micropolarity and dynamics of a matrix arranged in the regions where catalytic processes are carried out (50).

EPR spectroscopy is quite efficient in the study of structural and dynamics properties of various natural macromolecular systems, cellulose, and cotton fibers among them (51). Because a viscosity of various biopolymers is comparatively high, PC introduced into their bulk can move with correlation time $\tau_c \geq 10^{-9}$ s (21b). Anisotropic magnetic parameters of such PC and inhomogeneity of biopolymers should be taken into account. Therefore, the detailed study of structural and dynamics parameters of spin-labeled biopolymers requires the analysis of all their spectral components that become possible at millimeter wavebands EPR. It is demonstrated below by structural and dynamics investigation of cotton fibers 5595-V and microcrystalline cellulose modified by nitroxide radical at X- and D-bands EPR (23c,d,52).

D-band EPR spectra of these spin-modified biopolymers and the change in respective spectral components upon heating are presented in Figures 7 and 8, respectively. They are characterized by the considerable broadening of the canonic components caused by the interaction of the nitroxide fragment with hydroxyl groups of proteins. The magnetic resonance parameters of spin labels covalently attached to the cotton and cellulose macromolecules were determined as follows: $g_{xx} = 2.00842$, $g_{xx} = 2.00592$, $g_{xx} = 2.00224$, $A_{zz} = 3.76$ mT; and $g_{xx} = 2.00762$, $g_{xx} = 2.00582$, $g_{xx} = 2.00211$, $A_{zz} = 3.37$ mT, respectively. Comparative analysis allowed concluding that both the effective structure and polarity of the microenvironment of the radical, for example, in cotton are close to those in water. The same characteristics of the cellulose macromolecules were analyzed to be close to those in ethanol.

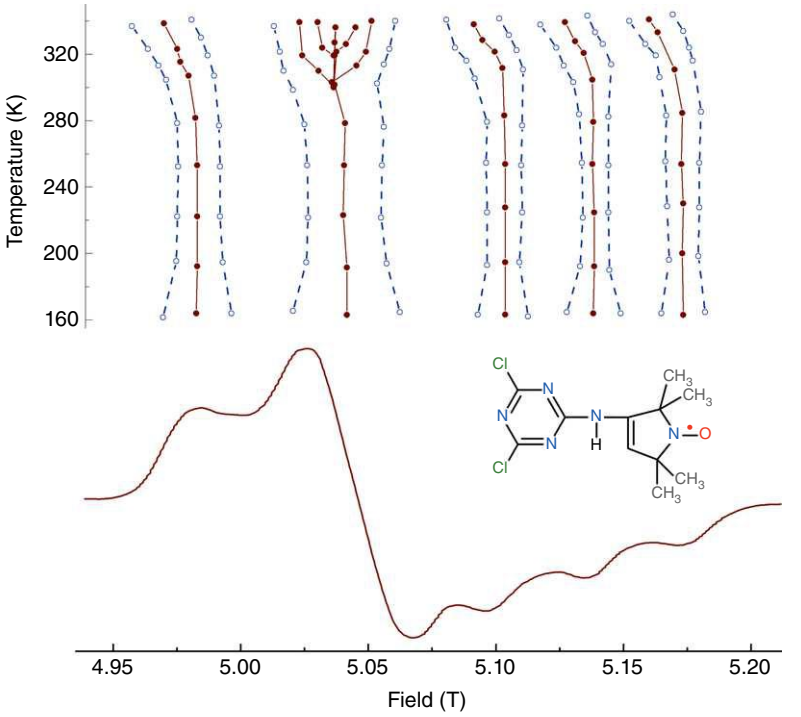

Fig. 7. D-band EPR spectrum of nitroxide radicals covalently attached to the chains of lyophilized cotton fiber 5595-V (below). The shift and broadening of spectral components with the sample heating are shown above by the solid and dashed lines, respectively.

When the samples are heated, the x-component of their EPR spectra shifts to high fields (Figs. 7 and 8). This is accompanied by partially eliminated of an initial inhomogeneous broadening of spectral components. It should be caused by the attenuation of the hydrogen bond between the radical NO-fragment and environmental molecules and/or by the defrosting of molecular mobility with correlation time of $\tau_c \leq 10^{-4}$ s in the place of label location. The spectral y-component of the 5595-V sample transforms at 315 K to a superposition of at least two lines, namely a wide singlet and a triplet with $g = 2.00610$ and $a = 1.52$ mT (Fig. 7). The latter contribution is due to the presence of small amount (~2%) of amorphous domains in which high radical mobility ($\tau_c \leq 2.2 \times 10^{-10}$ s at 335 K) occurs. The difference in isotropic g-factors of a spin label in the crystalline ($g_{iso} = 2.00553$) and amorphous ($g_{iso} = 2.00610$) phases agrees with the shift of spectral x-component to lower fields at the temperature increases and confirms that the acceleration of molecular motion in the amorphous domains of 5595-V sample is accompanied by the weakening of radical interaction with own microenvironment. The heating of the sample results in the shift and broadening of its spectral z components by 0.7 and 0.08 mT, respectively (Fig. 7). Such a weak broadening of the line accompanied by a considerable shift can be due to the Brownian isotropic rotation and hopping by arbitrary angles (53) or/and by the librations of the radical fragment (54) with the frequency of 10^9 s^{-1} and angular amplitude of $10^\circ \pm 3^\circ$ at 335 K.

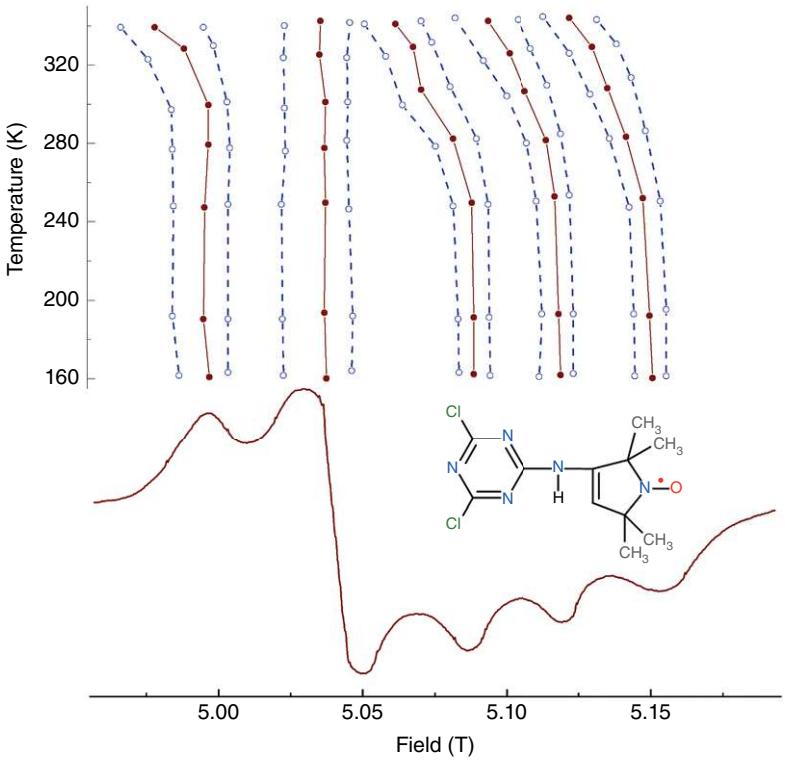

Fig. 8. D-band EPR spectrum of nitroxide radicals covalently attached to the chains of lyophilized microcrystalline cellulose (below). The shift and broadening of spectral components with the sample heating are shown above by the solid and dashed lines, respectively.

In cellulose, the only one type of domains was found. Its D-band EPR spectrum also demonstrates a shift of the z component toward g_{iso} at $T \geq 200$ K and the broadening at lower temperatures (Fig. 8). The analysis of the data presented concludes that Brownian rotation of spin label is realized around the axis lying at the molecular xz plane with $\tau_c = 5.8 \times 10^{-11}\exp(0.19\ \text{eV}/k_B T)$. Radical dynamics are defined by the shape of radical and the cavity in cellulose where it moves. Effective microviscosity η of such a cavity calculated from equation (8) with $r_{NO} = 0.2$ nm yields 11.2 Pa s at $T = 300$ K. Thus, the method allows to determine the elasticity of polymer matrix, the size of a cavity in its bulk where the radical moves.

More detailed information about structural and morphological properties of the macromolecular systems can be obtained from the multifrequency EPR study of PC formed upon their irradiation with photons of different energies. Figure 9 shows X- and D-bands EPR spectra of γ-irradiated cellulose obtained at room temperature (52b). The comparison of the spectra presented leads to the conclusion that at least three different PC are formed in γ-irradiated cellulose, namely singlet R_1 with $g_1 = 2.00281$, doublet R_2 $g_2 = 2.00295$ and $a_2 = 2.9$ mT, and triplet R_3 $g_3 = 2.00442$ and $a_3 = 2.7$ mT. Such an interpretation is consistent with the results obtained theoretically (55). The R_1 line can be attributed to contamination of lignin, whereas the formation of R_2 and R_3 centers can be explained by

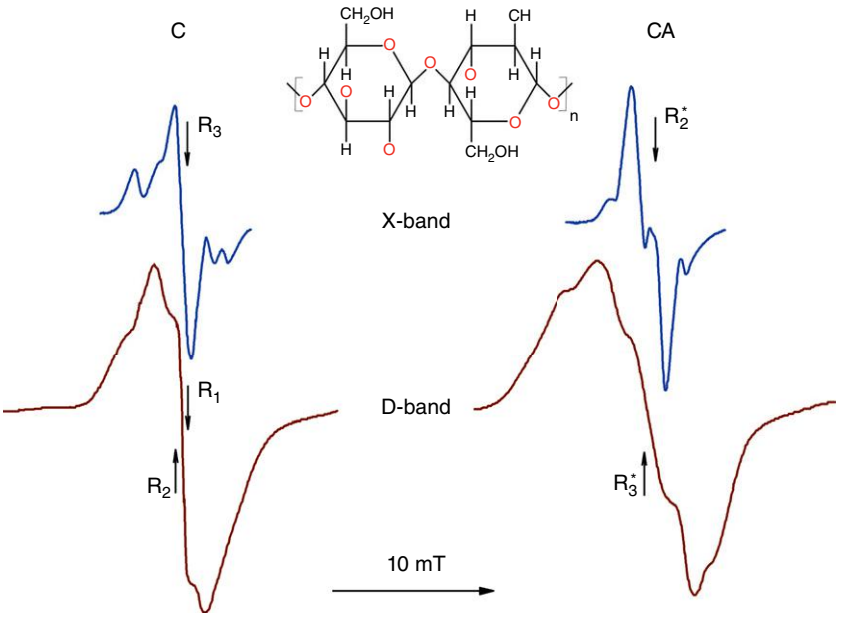

Fig. 9. X-band (above) and D-band (below) EPR absorption spectra of γ-irradiated (^{60}Co source, dose 0.1 MGy, 290 K) in air lyophilized cellulose (**C**) and that additionally amorphized under 2×10^9 Pa pressure between the Bridgeman anvils with 400^0 shift (**CA**).

dehydrogenation of the glucopyranose cycle in C_1 and C_4 positions, respectively. If the sample is previously amorphized under pressure (2×10^9 Pa) between the Bridgeman anvils (56) with 400° shift, at least two additional PCs appear in irradiated cellulose, namely doublet R_2^* with $g_2^* = 2.00505$ and $a_2^* = 1.5$ mT and triplet R_3^* with $g_3^* = 2.00532$ and $a_3^* = 2.2$ mT (Fig. 9). These PC were attributed to dehydrogenation of a glucopyranose cycle in the C_1 and C_4 positions, respectively. The effective relaxation time $\tau = \sqrt{T_1 T_2}$ (here T_1 and T_2 are the spin–lattice and spin–spin relaxation times, respectively) of these PC was determined from their MW-saturated EPR spectra. Such a parameter was obtained for both the R_3 and R_3^* to be $\tau_3 \geq 10^{-5}$ s and $\tau_3^* \geq 10^{-4}$ s, respectively. The correlation time of radical rotation in an amorphized sample, and its effective microviscosity was determined from respective D-band EPR spectra to be $\tau_c^* = 5.4 \times 10^{-13} \exp(0.32 \text{ eV}/k_B T)$ s and $\eta = 15.9$ Pa s, respectively. This evidences that cellulose amorphization increases the matrix rigidity in the place of PC localization and changes the morphology of a part of its subunits. This process is accompanied by the decrease in an interaction between PC and, therefore, by slowing down of their electron relaxation.

5. Conjugated Polymers

5.1. Polypyrrole. PP is a conjugated polymer widely investigated as a perspective molecular system for plastic electronics (57). The local ordering of PP is determined by the preparation method and crystallinity which can reach ~50%

(58). In contrast to PANI, the local order in the disordered phase of PP does not resemble that in the ordered regions.

Neutral PP exhibits a complex X-band EPR spectrum with a superposition of a narrow (0.04 mT) and a wide (0.28 mT) lines, both registered at $g \approx 2.0026$ (47,59), typical of PC formed in polyene and aromatic π-systems. The intensity of both lines corresponds to one spin per few hundred monomer units. A PP sample doped with oxidants exhibits only a strong narrow (~0.03 mT) X-band EPR spectrum with $g = 2.0028$ (47). Magnetic susceptibility of PC in a doped PP follows to Curie's law, and the charge is transferred according to the variable range hopping (VRH) model (60). The linewidth of PC stabilized in partly stretch-oriented PP was observed (61) as a function of temperature and the orientation of the sample in static magnetic field. As the oxygen molecules penetrate into the PP bulk, its EPR spectrum is broadened due to the exchange interaction of polarons with oxygen biradicals (62). Electron relaxation of PC in PP was shown (63) to depend on its doping level y. At a high y value, the susceptibility becomes Pauli-like and the polaron band observed in the PP optical spectrum due to the formation of spinless bipolarons (64). Thus, EPR signal of the doped PP is mainly attributed to neutral radicals and therefore reports little about the intrinsic conjugated processes. In this case, the method of spin probe described above becomes more effective in the study of structural and electronic properties of this conjugated polymer. PP labeled by the nitroxide radical during electrochemical synthesis was studied at X-band EPR by Winter and co-workers (65). However, effective spectrum of the sample did not contain lines of the probe possibly due to a high concentration of a spin probe introduced into PP.

Figure 10 exhibits X- and D-bands EPR spectra of a 2,2,6,6-tetramethyl-l-oxypiperid-4-yl-acetic acid introduced as a spin probe and also as a counterion into PP. Dashed lines show the spectra of the probe dissolved in nonpolar toluene (43). One can see in Figure 10**a** that at the X-band EPR the lines of the nitroxide radical rotating with correlation time $\tau_c > 10^{-7}$ s overlap with the single line of PC (R) localized in PP. Such an overlapping originating from a low spectral resolution hinders the separate determination of magnetic resonance parameters of these radicals and their spectral components.

The spectra of both the model and spin-modified polymer systems become predictably more informative at D-band EPR (Fig. 10**b**). At this waveband, all canonic components of EPR spectra of the probe in PP and toluene are completely resolved so that all the main terms of its $\boldsymbol{g}$ and $\boldsymbol{A}$ tensors can be measured directly. Nevertheless, the asymmetric spectrum of radicals R with magnetic parameters $g^R_{||} = 2.00380$, $g^R_{\perp} = 2.00235$, and $\Delta B_{pp} = 0.57$ mT is registered in the z-component of the probe spectrum. The nitroxide radical introduced into the nonpolar model system is characterized by the following magnetic resonance parameters: $g_{xx} = 2.00987, g_{yy} = 2.00637, g_{zz} = 2.00233; A_{xx} = A_{yy} = 0.60$ mT and $A_{zz} = 3.31$ mT. The difference $\Delta g = g^R_{||} - g^R_{\perp} = 1.45 \times 10^{-3}$ corresponds to an excited electron configuration in R with $\Delta E_{\sigma\pi^*} = 5.1$ eV lying near to an energy of electron excitation in neutral PPP. Once the probe is carried into the bulk of conducting PP, its g_{xx} value decreases down to 2.00906 and its spectral x- and y-components are broadened by $\delta(\Delta B_{pp}) = 4$ mT (Fig. 10**b**). Besides, the shape of the probe spectrum shows the localization of PC R in the polymer pocket of 1 nm size. This means

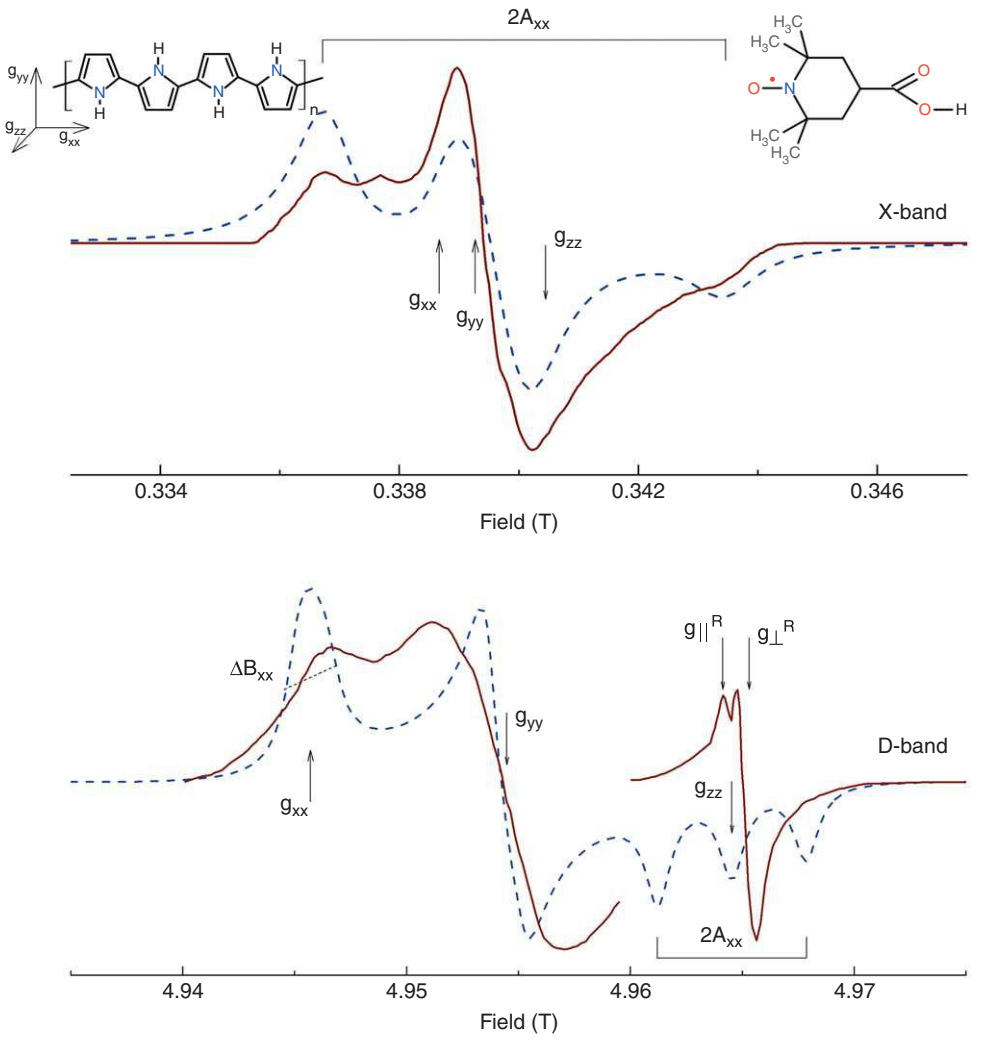

Fig. 10. The X-band (**a**) and D-band (**b**) absorption spectra EPR of 2,2,6,6-tetramethyl-l-oxypiperid-4-yl-acetic acid introduced as a spin probe into frozen (120 K) toluene (dotted line) and conductive PP (solid line). The anisotropic spectrum of localized paramagnetic centers marked by the symbol *R* and taken at a smaller amplification is also shown in the lower part of the figure. The measured magnetic parameters of the probe and radical *R* are shown.

that the charge is transferred by spinless bipolarons in doped PP, as it was proposed in the case of some other conducting polymers (23e,h,42c). Coulombic interaction of the probe active fragment with the extended spinless bipolarons causes the change in its magnetic parameters. The effective electric dipole moment of bipolarons diffusing near the probe was determined from the shift of the g_{xx} component to be equal to μ_v = 2.3 D. The shift of the **g** tensor term g_{xx} of the probe may be calculated within the frames of the electrostatic interaction of the probe and bipolaron dipoles by using the following approach.

Bipolaron induces in the place of the probe localization electric field with potential (66):

$$E_{\mathrm{d}} = \frac{k_{\mathrm{B}}T(x\coth x - 1)}{\mu_u} \tag{9}$$

where $x = 2\mu_u\mu_v(\pi\varepsilon\varepsilon_0 k_{\mathrm{B}}Tr^3)^{-1}$, μ_u is the dipole moment of the probe, ε and ε_0 are the dielectric constants for PP and vacuum, respectively, and r is the distance between the radical NO fragment and bipolaron. An isotropic hyperfine constant of the probe increases in this electrostatic field by the value $\Delta a_{\mathrm{iso}} = 7.3er_{\mathrm{NO}}t_{\mathrm{cc}}^{-1}$ (here t_{cc} is the resonant overlapping integral of C=C bond) and $dg_{xx}/dA_{zz} = 2.3 \times 10^{-2}$ mT^{-1} for such nitroxide radical (23c,d), one can write $\Delta g_{xx} = 6 \times 10^{-3}er_{\mathrm{NO}}k_{\mathrm{B}}T(x\coth x - 1)/(t_{\mathrm{cc}}\mu_{\mathrm{u}})$. By using $\mu_u = 2.7$ D (67), $\mu_v = 2.3$ D, and $r_{\mathrm{NO}} = 0.13$ nm (16,68), the value of $r = 0.92$ nm is obtained. The characteristic time τ_{c} of dipole–dipole interaction was calculated from the broadening of the spectral lines as described above to be $\tau_{\mathrm{c}} = 8.1 \times 10^{-11}$ s (43). This value is approximately equal to the polaron interchain hopping time, $\tau_{3\mathrm{D}} \cong 1.1 \times 10^{-10}$ s estimated for lightly doped PP (63b). The average time between the translating jumps of charge carriers is defined by the diffusion coefficient D and by the average jump distance equal to a product of lattice constant $d_{1\mathrm{D}}$ on halfwidth of charge carrier $N_{\mathrm{p}}/2$, $\tau = 1.5\langle d_{1\mathrm{D}}^2 N_{\mathrm{p}}^2\rangle/D$. Combining these dependences and using $D = 5 \times 10^{-7}$ m^2/s typical for conjugated polymers, one can determine $\langle d_{1\mathrm{D}}N_{\mathrm{p}}\rangle = 3$ nm approximately equal to four PP units.

Thus, the shape of the probe spectrum evidences a very slow motion of the probe due to a high molecular packing in PP. The interaction between spinless charge carriers with an active fragment of the probe results in the redistribution of the spin density between *N* and *O* nuclei in the probe and therefore in the change in its magnetic resonance parameters. The method also allows to evaluate characteristic size of a cavity in which the probe is localized and, therefore, the morphology of the sample under study. This makes it possible to determine the distance between the radical and the chain occupied by bipolaron and then the length and mobility of the latter.

5.2. Polytetrathiafulvalene. In recent decades, the electron donor tetrathiafulvalene (TTF) and its derivatives have been a subject of chemical and physical studies, due to the fact that many compounds of this group can form electrically conjugated charge transfer salts (69). To design conjugated TTF-based polymers more suitable for elements of molecular electronics, for example, diodes and chemical sensors (70), different polytetrathiafulvalene (PTTF) samples were synthesized. PTTF in which TTF units are linked by phenyl or tetrahydroanthracene bridges is a p-semiconductor with the highest conductivity $\sigma_{\mathrm{dc}} \approx 0.1$–0.01 S/m (71). Charge transport in the polymers can be described in terms of a VRH and a thermally activated hopping at low and high temperature regions, respectively (72). EPR and Mössbauer measurements of doped PTTF indicate a polaron–bipolaron charge transfer mechanisms whose contributions are determined by the doping level *y* and temperature (73).

The nature, composition, and dynamics of PC in these initial and iodine-doped PTTF samples were studied in detail by the multifrequency EPR method

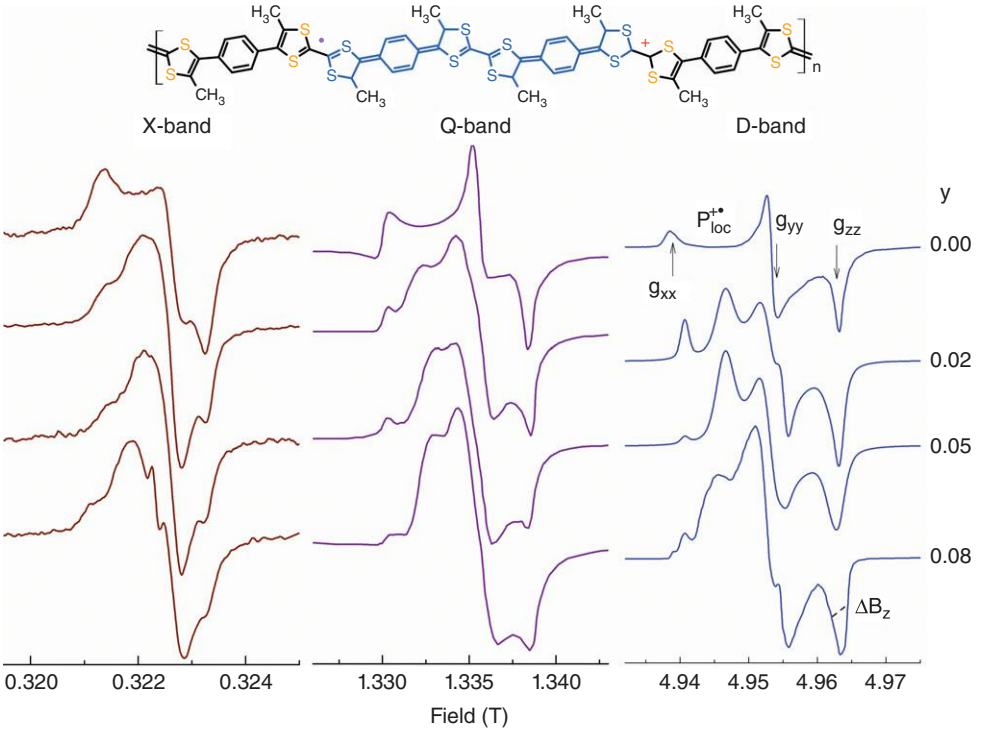

Fig. 11. Typical in-phase X-, K-, and D-bands absorption spectra EPR of the initial and differently iodine-doped PTTF-CH_3—C_6H_4 samples registered at room temperature. The measured magnetic parameters are shown.

(42a–c). Figure 11 exhibits exemplary spectra of the different iodine-doped PTTF-CH_3—C_6H_4 sample obtained at various EPR wavebands. This allows one to separate and measure more correctly all terms of the anisotropic magnetic resonance parameters of polarons with different mobility. The analysis of the data presented showed that EPR spectrum of the sample contains contributions of localized polarons $P^{+\bullet}_{loc}$ with slowly temperature-dependent magnetic parameters g_{xx} = 2.01189, g_{yy} = 2.00544, g_{zz} = 2.00185, and more mobile PC $P^{\bullet+}_{mob}$ with g_{xx} = 2.00928, g_{yy} = 2.00632, g_{zz} = 2.00210. The concentrations ratio of these PCs in undoped powder is 20:1. The total number of polarons increases from 2×10^{17} cm^{-3} up to 3×10^{17} cm^{-3} at the polymer doping. The above terms of ***g***-tensor exceed the corresponding magnetic parameters of the polarons in PT (23e,h, 74) and its derivatives (25g,j,k). This indicates a stronger spin–orbit interaction of the spin with the nucleus of the sulfur atom in the PTTF backbone.

As the frequency of spin precession increases, the interaction between spin packets becomes slower. This provokes MW saturation of PC and appearance of bell-like terms in their dispersion or absorption EPR spectra (22). The first derivative of, for example, dispersion signal U is generally written as (75)

$$U(\omega t) = u_1 g^{|}(\omega)\sin(\omega t) + u_2 g(\omega)\sin(\omega_e t - \pi) + u_3 g(\omega)\sin(\omega t \pm \pi/2) \qquad (10)$$

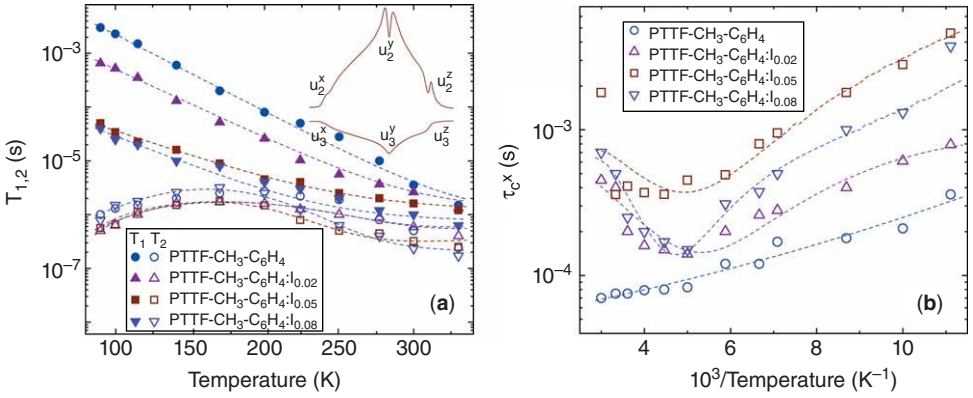

Fig. 12. (**a**) Temperature dependence of effective spin–lattice T_1 and spin–spin T_2 relaxation times of polarons in the initial and differently iodine-doped PTTF-CH_3—C_6H_4 sample determined from their in-phase (above) and π/2-out-of-phase (below) D-band dispersion spectra (inset). (**b**) Arrhenius dependencies of correlation time τ_c^x of x-anisotropic libration of polarons localized on the initial and differently iodine-doped PTTF chains evaluated from its π/2-out-of-phase dispersion spectral term u_3.

where u_1, u_2, and u_3 are the in-phase and π/2-out-of-phase dispersion terms, respectively, and $g(\omega)$ is a factor of line shape. $\omega_m T_1 > 1$ inequality is realized for an undoped PTTF sample, so that the first derivation of its dispersion signal is determined mainly by the u_2 and u_3 terms of equation (10) (see insert of Fig. 12**a**). On the other hand, $\omega_m T_1 < 1$ condition is actual for slightly doped polymer; therefore, its dispersion term is determined by u_1 and u_3 terms of the above equation. The u_i^x, u_i^y, and u_i^z terms of undoped sample are registered at $g_{xx} = 2.01189, g_{yy} = 2.00564$, $g_{zz} = 2.00185$.

Earlier, it was shown (36,76) that spin relaxation and dynamics parameters of PC adiabatically saturated in conjugated polymers can be determined separately from the analysis of both the in-phase and out-of-phase dispersion spectral components.

The temperature dependencies of effective relaxation times T_1 and T_2 of polarons determined from relation of the u_1, u_2, and u_3 terms of the PTTF-CH_3-C_6H_4 sample are shown in Figure 12**a**. The T_1 value of the sample changes with the temperature as $T^{-\alpha}$ with α lying near 3 and 5 for mobile and pinned polarons, respectively. Such a difference in α can be caused, for example, by an interaction of respective charge carriers with own microenvironment.

Macromolecular motion in polymers is *a priori* strongly anisotropic carrying out with the correlation time $\tau_c \geq 10^7$ s^{-1}. Such dynamics is studied by using the ST-EPR method (22), which becomes more informative at D-band EPR (42a,b). It was shown that the heating of PTTF sample results in an increase of the ratio u_3^x/u_3^y parameter due to superslow librations of polarons pinned near main x-axis of the polymer chains. The Arrhenius dependencies of correlation times of such dynamics in PTTF samples with different doping level are shown in Figure 12**b**. Extrapolation to the low-temperature range allows one to estimate the maximum value of τ_c is ca. 10^{-4} s at $T = 75$ K when $u_3^x/u_3^y = 0.07$. Once the initial sample is

doped up to $y = 0.02$, 0.05, and 0.08 levels, the energy E_a required for activation of the macromolecular motion increases from 0.019 up to 0.023 to 0.033 and to 0.036 eV, respectively. E_a values obtained at D-band EPR are comparable with those determined at lower registration frequency for interchain charge transfer in doped PTTF (71, 73b) that indicates the interaction of pinned and mobile polarons in this polymer matrix.

To compare experimental results with the polaron theory, Q1D diffusion motion of mobile PC along and between PTTF's chains with the diffusion coefficients D_{1D} and D_{3D}, respectively, was assumed.

The diffusion of electron spins along and between polymer chains induces a local magnetic field, fluctuating rapidly with time near the location of another electron spins due to their dipole–dipole interaction. Such an interaction accelerates spin relaxation, so that one can write the following relations of the relaxation and dynamics parameters of polarons diffusing in a real polycrystalline system (77):

$$T_1^{-1} = \langle \Delta\omega^2 \rangle \left[2J(\omega_e) + 8J(2\omega_e) \right] \tag{11}$$

$$T_2^{-1} = \langle \Delta\omega^2 \rangle \left[3J(0) + 5J(\omega_e) + 2J(2\omega_e) \right] \tag{12}$$

where $\langle \omega^2 \rangle = 1/10\gamma_e^4\hbar^2 S(S+1)n\Sigma_{ij}$ is a constant of dipole–dipole interaction for powder, γ_e is a hyromagnetic ratio for electron, n is a number of polarons per each monomer, Σ_{ij} is a lattice sum for powder-like sample, $J(\omega) = (2D_{1D}^{|}\omega)^{-1/2}$ (at $D_{1D}^{|} >> \omega >> D_{3D}$), $J(0) = (2D_{1D}^{|}D_{3D})^{-1/2}$ (at $D_{3D} >> \omega$) is a spectral density function for polaron longitudinal diffusion at first (ω_e) and second ($2\omega_e$) resonant angular frequency of the electron spin precession, respectively, $D_{1D}^{|} = 4D_{1D}/L^2$, and L is a factor of spin delocalization over a polaron. It should be noted that a spectral density function for spin rotational dynamics with correlation time τ_c and coefficient $D_{rot} = 1/6\tau_c$ is $J(\omega) = \tau_c/(1 + \tau_c^2\omega^2)$.

The temperature dependencies of effective D_{1D} and D_{3D} calculated for PC in different PTTF samples by using equations (11) and (12) and the data presented in Figure 12**a** are shown in Figure 13. It is observed from the figure that the value of D_{1D} does not exceed 2×10^{12} rad/s for PTTF samples at room temperature. This parameter is at least two orders of magnitude lower than that obtained for polarons in PP (78) and PANI (5b) at lower ω_e.

The Fermi velocity v_F determined for PTTF samples was near to 1.9×10^5 m/s (42c). The mean free path l_i of a charge carrier diffusing along polymer chain with the lattice constant c_{1D} can be evaluated as $l_i = D_{1D}c_{1D}^2/2\pi v_F = 10^{-2}$–$10^{-4}$ nm for the PTTF samples. This value is less than the lattice constant a; therefore, the charge is transferred incoherently in this polymer, which cannot be considered as a Q1D metal. For such a case, the interchain charge transfer integral can be determined as (79) $t_\perp = v_F\hbar/2a = 0.05$ eV. This value lies near to activation energies of chain librations and interchain polaron hopping in a doped PTTF-CH_3—C_6H_4 sample. These facts indicate that the charge transfer in a polymer is governed mainly by interchain phonon-assisted polaron hopping, which is stimulated by macromolecular dynamics. This evidences for the interaction of molecular and charge dynamics in PTTF. It also confirms the supposition (80) that the

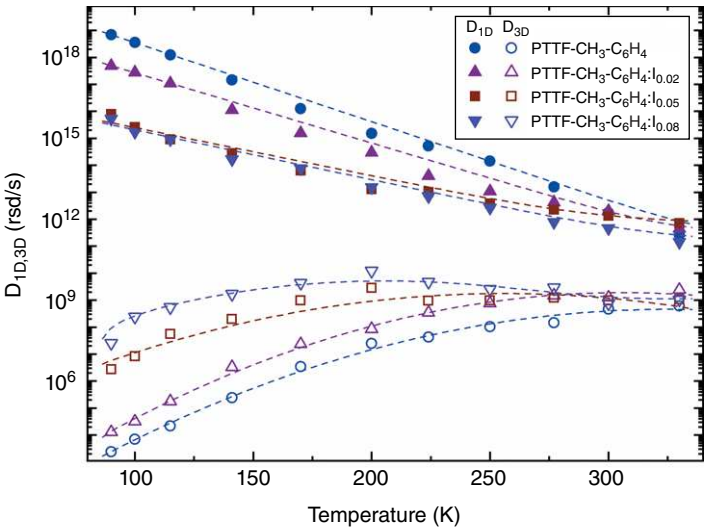

Fig. 13. Temperature dependencies of the polaron intrachain D_{1D} and interchain D_{3D} diffusion coefficients determined for the PTTF-CH_3—C_6H_4 sample from equations (11) and (12) and the data presented in Figure 12**a**.

fluctuations of lattice oscillations, librations among them, can modulate the electron interchain transfer integral in such conjugated compounds.

The rise of libron–exciton interactions at the PTTF doping evidences the formation in polymer matrix of a complex quasi-particles, namely molecular–lattice polarons (81). According to this phenomenological model, molecular polarons are additionally covered by lattice polarization, so that their mobility becomes as a sum of mobilities of molecular and lattice polarons. The energy of formation of such molecular–lattice polarons E_p in PTTF was determined to be 0.19 eV (42a). The characteristic time, necessary for polarization of both atomic and molecular orbitals of polymer can be determined as $\tau_p \approx \hbar E_p = 3.5 \times 10^{-15}$ s. This value is more than two orders of magnitude less than intra- and interchain hopping times for charge carriers in PTTF (Fig. 13). This leads to the conclusion that the time τ_h required for the hopping of charge carriers in PTTF sufficiently exceeds the polarization time for charge carriers' microenvironment in the polymer, that is $\tau_h >> \tau_p$. This inequality is a necessary and sufficient condition for electronic polarization of polymer chains by charge carriers.

5.3. Poly(3-octylthiophene). Regioregular poly(3-alkylthiophenes) (P3AT) were shown (82) to be suitable sulfur-based Q1D system for the design of respective molecular electronic and optical applications. Undoped P3AT are semiconductors, and their energy bandgap (~2 eV) is determined by the presence of the π-orbital conjugation along the main polymer axis. The maximum σ_{dc} value of I_2-doped poly(3-hexylthiophene) (P3HT), poly(3-octylthiophene) (P3OT), and P3DDT is 6×10^3, 2×10^4, and 1×10^5 S/m, respectively, at room temperature (83). This shows the correlation of a charge transport with the length of alkyl groups and the morphology of the sample. Charge dynamics can also be governed by the presence in this class of materials of positively charged mobile polarons

originated from the synthesis and/or the adsorption of oxygen from ambient atmosphere (spontaneous *p*-type doping) (84). At higher doping level *y*, the polarons combine to form diamagnetic bipolarons like it happened in other π-conjugated polymers (see Fig. 1). Polarons stabilized in P3AT possess spin $S = ½$ as well that also stipulates their detailed investigation by different magnetic resonance methods.

Regioregular P3OT is also used as active matrix of molecular devices, for example, chemical sensors (85) and polymer:fullerene solar cells (86). A constriction (8.2 meV/kbar) of the initial P3OT bandgap (2.02 eV) was observed (87) due to the decrease of the torsion angle between its adjacent thiophene rings and the enhancement of interchain interactions between parallel polymer planes. More detailed information on the magnetic and electronic properties of the initial and treated P3OT sample was obtained at X- and D-bands EPR (88).

Figure 14 shows EPR spectra of regioregular P3OT sample obtained at both wavebands EPR at room temperature. At the X-band, the samples show a single nearly Lorentzian EPR line with $g_{\text{eff}} = 2.0019$, $\Delta B_{\text{pp}} = 0.27$ mT, and spin concentration 3.9×10^{25} m^{-3} or 0.013 spin per a monomer unit. At the D-band EPR, the samples demonstrate the superposition of more broadened convoluted Gaussian and Lorentzian lines (with the Lorentzian/Gaussian line shape ratio ca. 0.4) with the anisotropic *g*-factor (Fig. 14**c**) as it is typical for PC in some other conjugated polymers with heteroatoms. The main components of its **g** tensor were determined from this spectrum to be $g_{xx} = 2.00409$, $g_{yy} = 2.00332$, and $g_{zz} = 2.00235$. The effective *g*-factor of the P3AT is higher than that of most hydrocarbonic conjugated polymers; therefore, one can conclude that in P3AT the unpaired electron interacts with sulfur atoms. This is typical for other sulfur-containing compounds (23g,42c,89) in which sulfur atoms are involved into the conjugation.

Figure 15 evidences that the g_{xx} and g_{yy} values of polarons stabilized in the P3OT decrease with the temperature decrease from 333 to 280 K possibly due to the transition to the more planar conformation of the polymer chains. Below 280 K, these values increase at the sample freezing down to 160–220 K and then start to decrease at the further drop in temperature. The decrease of g_{xx} and g_{yy} values at low temperatures can be explained by a libration of macromolecules which is evoked by modulation of the crystal field.

The linewidth of the spectra increases by a factor of ca. three at the increase of the spin precession frequency due to Gaussian distribution of PC with slightly anisotropic magnetic parameters. Figure 15 also presents temperature dependence of the linewidths of all canonic spectral components. It is seen that these parameters first increases with the temperature increase from 90 K up to some characteristic temperature $T_{\text{c}} = 170$–210 K and then decreases at the further increase in temperature. These dependences can be described in the framework of the dipole–dipole exchange interaction of mobile polarons hopping in a polymer network (23g, 25j). Such an interaction should broaden the spectral lines by an amount (90):

$$\delta(\Delta\omega) = p_{\text{ff}}\omega_{\text{hop}}n_{\text{g}} \tag{13}$$

where $p_{\text{ff}} = 16/27\alpha^2/(1+\alpha^2)$ is the probability of spin flip-flop during a collision, $\alpha = (3/2)\ 2\pi J_{\text{ex}}/\hbar\omega_{\text{hop}}$, J_{ex} is the constant of exchange spin interaction,

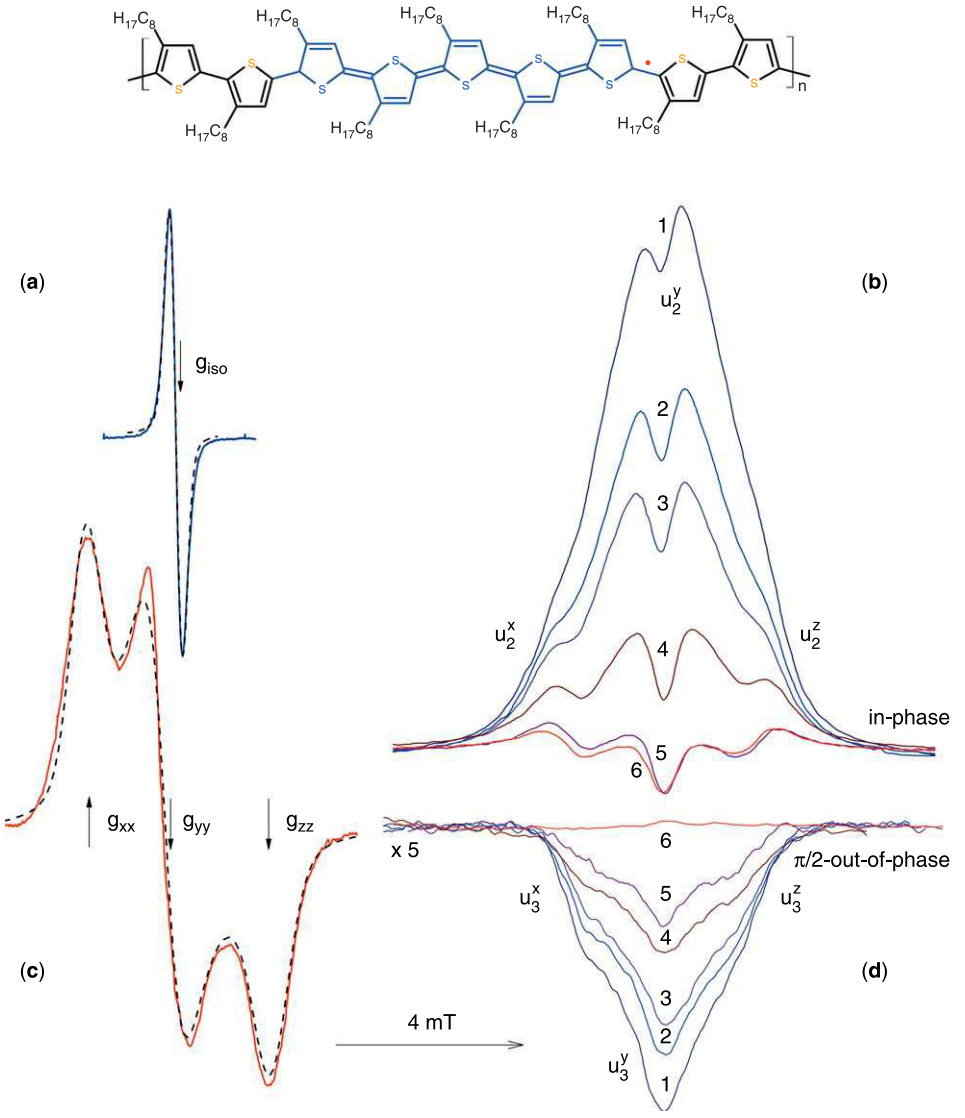

Fig. 14. X-band (**a**) and D-band (**b**–**d**) absorption (**a**,**c**) and in-phase (**b**) and $\pi/2$-out-of-phase (**d**) dispersion spectra EPR of regioregular poly(3-octylthiophene) obtained at room temperature (**a**,**c**) and 90 (1), 100 (2), 110 (3), 145 (4), 200 (5), and 250 K (6). The terms of anisotropic magnetic parameters are shown.

$\omega_{hop} = \omega^0_{hop}\exp(-E_a/k_BT)$ is the frequency of polaron hopping, and n_g is the guest PC number per each polymer unit. Extreme forms of the dependences should evidence the realization of strong and weak spin exchange interaction at $T \leq T_c$ and $T \geq T_c$, respectively. An additional reason of the line broadening can be the spin trapping at the lower temperature T_c. The change in the width of the x-, y-, and z-spectral components made it possible to obtain the value $E_a = 0.0215$,

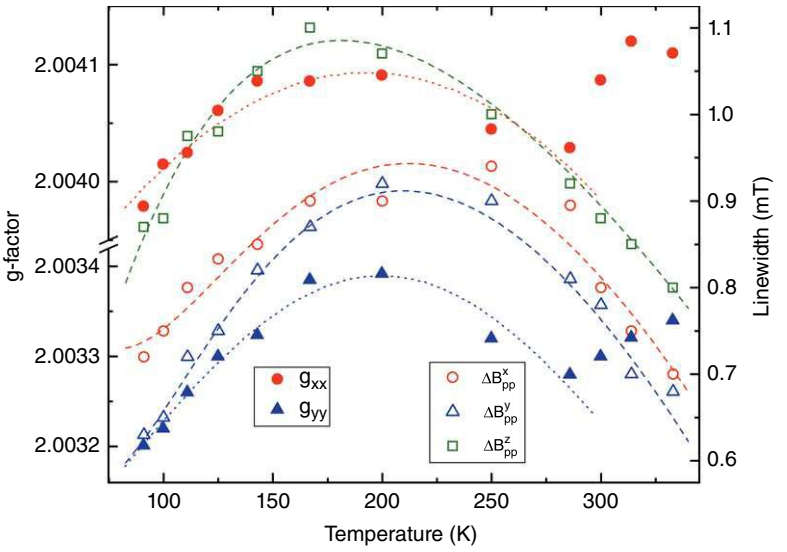

Fig. 15. Temperature dependences of the main terms of anisotropic g-factor and linewidth of regioregular poly(3-octylthiophene) determined at D-band EPR. The respective functions calculated theoretically are shown by dotted and dashed lines, respectively.

0.0186, and 0.0096 eV, respectively, for polaron dynamics in respective regions of regioregular P3OT. The energies for activation of molecular motion near the principal macromolecular x-, y-, and z-axes were determined for the sample from equations (4) and (5) to be 3.6, 4.9, and 4.3 meV, respectively (88).

It is seen from Figure 15 that the respective terms of anisotropic magnetic parameters correlate at least at $T \leq T_c$. This indicates that various circumstances can affect the P3OT canonic spectral components, including the scattering of charge carriers on the polymer lattice phonons.

Figures 14**b** and 14**d** exhibit the in-phase and $\pi/2$-out-of-phase terms of D-band EPR dispersion spectra of P3OT registered at different temperatures. It is seen that the Gaussian bell-like contribution is included in both dispersion terms. The appearance of such a component is attributed to the adiabatically fast passage of saturated spin packets by a modulating magnetic field (22). Relative intensities of the $\pi/2$-out-of-phase spectral components change with the temperature. This effect evidences the appearance of the saturation transfer over the quadrature spectrum due to superslow macromolecular dynamics. Analyzing the dispersion spectral components, the times of electron relaxation and correlation of libration motion of the chain macromolecular segments near the principal molecular x-axis in P3OT were determined separately. The latter parameter, τ_c^x, of P3OT was obtained to characterize with complex temperature dependence with the special temperature point $T_c \approx 150$ K. It was interpreted in the frames of the superslow activation (with $E_a = 0.069$ eV) joint Q1D libration of polarons on polymer chains at $T \leq T_c$ and collective Q2D motion at $T \geq T_c$ (88). The upper limit for the correlation time of anisotropic molecular motion in the sample was evaluated to be $\tau_c^x \leq 4.4 \times 10^{-4}$ s at 66 K.

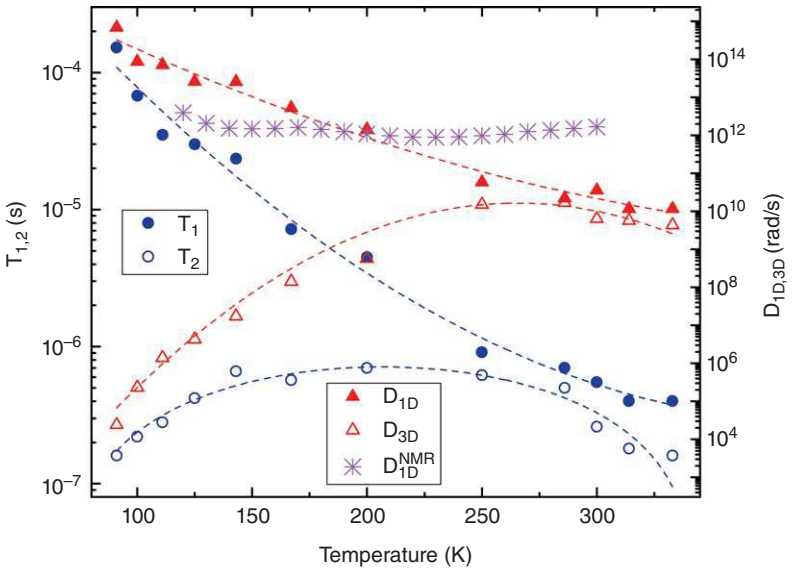

Fig. 16. Temperature dependences of the spin–lattice T_1 and spin–spin T_2 relaxation tomes as well as the coefficients of intrachain D_{1D} and interchain D_{1D} polaron dynamics in regioregular poly(3-octylthiophene) at D-band EPR. By the stars is shown the dependence $D_{1D}(T)$ obtained by the ^{1}H 50 MHz NMR method (see the text). By the lines are shown the dependences calculated theoretically. NMR $T_1(T)$ data were used for calculation the above dynamics parameter. Reprinted with permission from Ref. 92 . Copyright (1999) Elsevier.

Figure 16 exhibits the change of both relaxation times with the temperature. One can conclude from these data that as the temperature of the P3OT sample increases, its spin–lattice relaxation accelerates to the point that $T_1 \approx T_2$ at room temperature that is typical for other organic solids. As the precession frequency of polarons' spin increases in ca. 14 times at transition from X- to D-band EPR, the T_2 value of polarons stabilized in the P3OT sample increases by a factor of six. Such an effect can be explained in terms of modulation of spin relaxation by spin Q1D and Q3D dynamics in the polymer. In this case, both the electron relaxation times should vary as $T_{1,2} \propto \omega_e^{1/2}$ (91), that is it should change relaxation times by a factor of near four. Note that Q2D spin motion at such transition should lead to $T_{1,2} \propto \ln(\omega_e)$ dependency (91) and to the change in spin relaxation by factor of about two.

Figure 16 shows the temperature dependencies of the effective dynamic parameters D_{1D} and D_{3D} calculated from equations (11) and (12) with $L \approx 5$ (5b). The RT D_{3D} value obtained lies near $D \approx 2.1 \times 10^{10}$ rad/s evaluated from the charge carrier mobility in slightly doped P3OT (92). The RT anisotropy of spin dynamics D_{1D}/D_{3D} decreases from 2.9×10^{10} down to 3 at the sample heating within 90-330 K range that is typical for low-dimensional systems. $D_{1D}(T)$ dependence calculated from the ^{1}H 50 MHz spin–lattice relaxation data obtained by Masubuchi and co-workers (93) for the P3OT is also presented in Figure 16 for comparison. It is seen from the figure that the D_{1D} value calculated from the NMR data is changed with the temperature. Such discrepancy occurs probably because NMR

is rather an indirect method for studying electron spin dynamics in this and other conjugated polymers.

A strong temperature dependence of intrachain polaron dynamics can be described, as in case of other conjugated polymers (25j), in terms of polaron scattering on the phonons of crystalline lattice domains embedded into an amorphous polymer matrix. According to this model, such scattering should accelerate polaron intrachain diffusion by the value (94):

$$D_{1D}(T) = D_{1D}^{(0)} T^2 \cdot \left[\sinh\left(\frac{E_{ph}}{k_B T} \right) - 1 \right] \tag{14}$$

where E_{ph} is the energy of lattice phonons. Indeed, it is seen from Figure 16 that the data experimentally obtained are fitted well by equation (14) with $E_{ph} = 0.13$ eV. This value lies near the energy of lattice phonons of various conjugated polymers (0.09–0.32 eV) (25j, 42c).

The temperature dependence for D_{3D} can be described in terms of the thermal activation of the charge carriers from widely separated localized states in the gap to closely localized states in the tails of the valence and conjugated bands (5b). Such an approach predicts the following diffusion coefficient for Q3D spin mobility:

$$D_{3D}(\omega_e T) = D_{3D}^{(0)} k_1 T^2 \omega_e^s \exp\left(\frac{E_b}{k_B T} \right) \tag{15}$$

where k_1 is constant, $s = 1$–6 $k_B T/E_b$ is the parameter reflecting polymer system dimensionality, and E_b is the energy required for spin crossing a barrier. The value E_b was determined for P3OT to be 0.18 eV, which lies near that obtained for some organic molecular conductors (69). The increase of the dimensionality of the polymer system should decrease E_b.

Thus, the interaction of the spin charge carriers with heteroatoms in sulfurous organic polymer semiconductor P3OT originates the anisotropy of its g-factor registered in its D-band EPR spectrum. Spin relaxation and dynamics are determined by the interaction of the mobile polaron with optical phonons of the polymer lattice. The near values of the energies of spin interchain transport, dipole–dipole interaction, and the optical lattice phonons indicate the correlation of charge transport and macromolecular dynamics in this polymer. It can be concluded that two types of charge transport mechanism can be associated with change in the lattice geometry at the characteristic (the polymer–glass transition) temperature T_c, for example, with its thermochromic effect.

Finally, let the possibilities of the method for investigating more complex multispin polymer systems is considered.

5.4. Polymer:Fullerene Nanocomposite. Conjugated polymers attract much interest also due to their perspective use as active matrix in photovoltaics (95). Main photoactive elements consist of polymer and fullerene subsystems which act as electron donor and acceptor, respectively. Once heterojunctions (BHJ) of such materials are illuminated, spinless excitons are first formed in their bulk. These quasi-particles can geminate ultrafast dissociate forming Coulomb bound electron–hole pairs (charge-transfer states) of electrons

on the acceptor moiety and holes on the donor moiety. Then electrons and holes can leave the donor:acceptor interface relaxing into more favorable energy levels (96). With increasing distance from the material interface, the Coulomb attraction becomes so less that the electrons and holes become independent of each other and form respective charge-separated states. As a result, charge separation leads to the formation of unbound (free) positively charged polarons on polymer chains and negatively charged radical on fullerene molecules. After this stage, charge carrier recombination can occur. The separation and recombination of free charge carriers can be considered as concurring direct and backward-directed process. The geminate recombination of polaron–fullerene pairs is monomolecular and, therefore, a first-order process. The nongeminate, bimolecular recombination of separated polaron–fullerene pairs following Langevin theory of a second-order. This process is governed by the system structure and morphology. For example, the fluorination of a copolymer: fullerene composite improves its power conversion efficiency more than five times (97).

Because both the charge carriers possess a spin, their formation, dynamics and recombination are spin-assisted (96). This is why the direct light-induced EPR (LEPR) method became one of the most powerful method for the study of magnetic, relaxation, and dynamics processes carrying out in organic polymer:fullerene systems (15,25g,j,96,98). The possibilities of studying such systems by the EPR method are discussed below using the exemplar poly[*N*-9′-heptadecanyl-2,7-carbazole-alt-5,5-(4′,7′-di-2-thienyl-2′,1′,3′-benzothiadiazole)]:[6,6]-phenyl-C61-butyric acid methyl ester (PCDTBT:PC61BM) BHJ widely used in organic electronics and photonics (99). High efficiency of the energy conversion in the PCDTBT:PC61BM BHJ was explained (100) by its lowered, less than 1.9 eV (101), bandgap and "column-like" bilayer ordered copolymer matrix. Polarons and methanofullerene anion radicals in this composite are characterized by weakly anisotropic g-factors with g_{xx} = 2.00320, g_{yy} = 2.00240, g_{zz} = 2.00180 (5d), and g_{xx} = 2.00058, g_{yy} = 2.00045, g_{zz} = 1.99983 (102), respectively. The LEPR study of these charge carriers photoinitiated by photons with the energy of 1.32–3.14 eV showed (103) that upon illumination a part of spin charge carriers are fixed in trap sites whose number and depth are governed by a structure of the BHJ and an energy of the initiating photons. Exchange- and multitrap-assisted recombination of free charge carriers is governed by their dynamics as well as by structure and morphology of their microenvironment.

Figure 17**a** shows X-band LEPR spectrum of PCDTBT:$PC_{61}BM$ composite photoinitiated by photons with the energy $h\nu_{ph}$ = 2.38 eV at T = 77 K (103d,e). D-band LEPR spectrum reconstructed by differentiating the integral form of the corresponding spectrum obtained by Niklas and others (5d) at $h\nu_{ph}$ = 2.33 eV at T = 50 K is presented in Figure 17**b**. As in the case of analogous polymer: fullerene (25g,j) and copolymer: fullerene (25j) composites, these spectra were attributed to polarons photoinitiated on copolymer chains and $PC_{61}BM$ methanofullerene anion radicals situated between them registered. The spectra of these charge carriers are registered at lower and higher magnetic fields, respectively. To determine main magnetic resonance parameters of all radicals and to analyze their change with experimental conditions, the above sum LEPR spectra of the sample should be deconvoluted by using numerical simulation (5d,25j,102). Such an algorithm in combination with the "light on-light

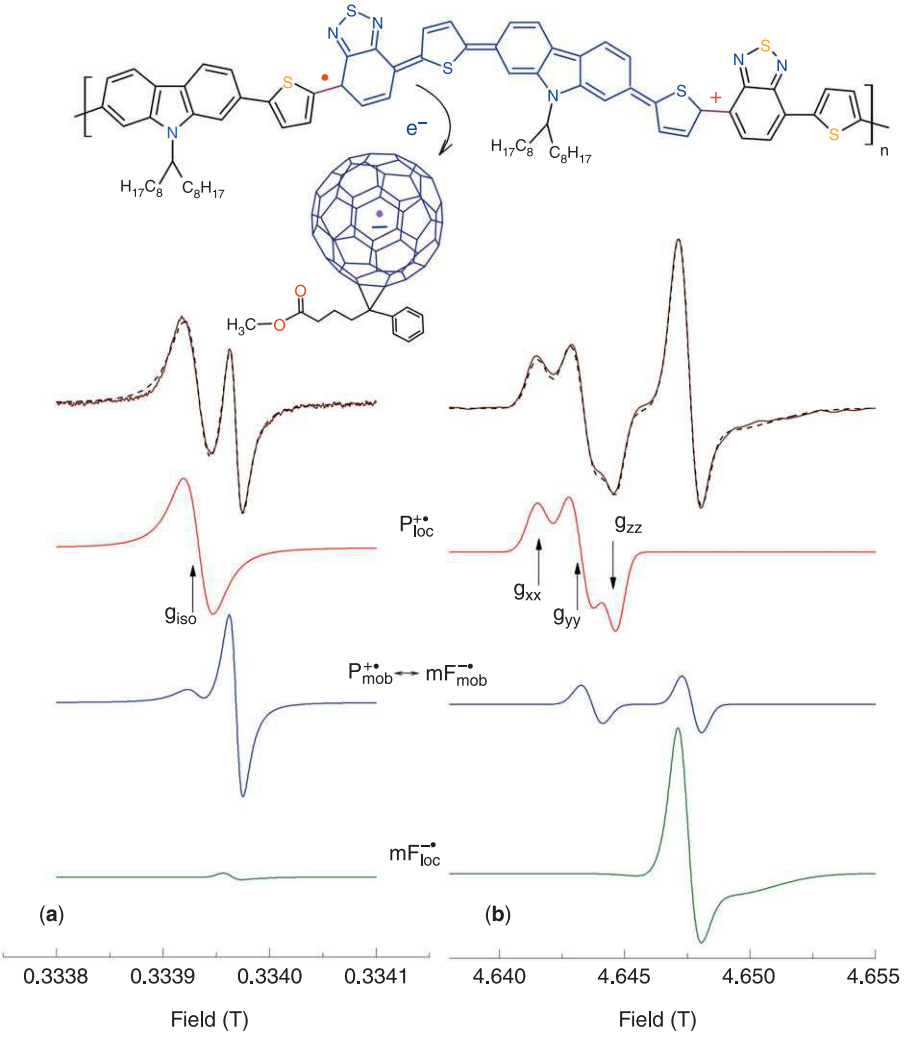

Fig. 17. X- (**a**) and D-band (**b**) LEPR spectra of polarons and methanofullerene charge carriers background photoinduced by photons with $h\nu ph$ = 2.34 eV at T = 77 and 50 K, respectively. Calculated sum spectra and their contributions caused by localized polarons $P^{+\bullet}_{loc}$, methanofullerene anion radicals $mF^{-\bullet}_{loc}$ and mobile radical pairs $P^{+\bullet}_{mob} \leftrightarrow mF^{-\bullet}_{mob}$ are shown as well. The charge transfer from a copolymer chain to a methanofullerene molecule accompanied by the formation on the copolymer chain of polaron with an elementary positive charge and spin S = ½ is shown schematically. Reconstructed D-band spectrum is shown. Reprinted with permission from Ref. 5d. Copyright (2013) The Royal Society of Chemistry.

off" method allowed to obtain separately all magnetic resonance parameters of both charge carriers. The figure depicts theoretically calculated sum spectra and their contributions due to mobile spin pairs of polarons and fullerene anion radicals $P^{+\bullet}_{mob} \leftrightarrow mF^{-\bullet}_{mob}$ as well as the same charge carriers pinned in copolymer spin traps, $P^{+\bullet}_{loc}$ and $mF^{-\bullet}_{loc}$.

By analyzing LEPR spectra, it becomes possible to separate the decay of mobile and pinned spin charge carriers excited in polymer matrix. Localized positive charge carriers can either be retrapped by vacant trap sites or recombined with opposite guest charges. Trapping and retrapping of polarons reduce their energy that results in their localization into deeper traps and in over time increase of number of localized polarons. It was shown (103d,e) that the spin decay process in the PCDTBT:$PC_{61}BM$ can be described in terms of Tachiya's approach (104) of charges in geminate recombination during their repeated trapping and detrapping from trap sites with different depths in energetically disordered semiconductors. Therefore, the decay of long-lived charge carriers originated from spin pairs photoinduced in these BHJ is strongly governed by the number and width of energy distribution of trap sites.

From the comparison of the spectra obtained at different wavebands, one can note the drastic increase of concentration of pinned radicals at higher spin precession frequency. This can be explained by an increase in the number and/or energy depth of the spin traps due to the interaction of spins with an external magnetic and/or MW field. If the initial excitons can be considered as relatively isolated quasi-particles, there should be a reasonably high probability that a metastable PC may result from the optical production of an electron–hole pairs by means of the trapping of their one carrier and the hopping away of the other (105). Such an interaction should suppress the charge transfer through BHJ with the increase of the electron spin precession frequency ω_e. Besides, the irradiation of the composites leads to the reversible formation of spin traps in their copolymer backbone. This changes (also reversibly) the properties of microenvironment of captured spins and, therefore, the energy of their resonant excitation on respective levels. The formation of such traps shows the dependence of the main magnetic resonance parameters of PC on the photon frequency and the number and depth of spin traps in the polymer matrix.

Figure 18**a** depicts the dependence of the relative concentration of polarons $P^{+\bullet}_{loc}$ and methanofullerene anion radicals $mF^{-\bullet}_{mob}$ in the PCDTBT:$PC_{61}BM$ composite on the energy of initiating photons $h\nu_{ph}$. One can note that two main types of the data are presented. The first is the higher relative concentration of localized carriers in comparison with that of mobile PC. Another feature is the nonmonotonic dependence of the number of both charge carriers on the photon energy. As shown in Figure 18, the number of both the charge carriers is characterized by dependence with explicit extremes lying near 1.8 and 2.8 eV. The analogous dependences were also obtained for both charge carriers photoinitiated in the PCDTBT:$PC_{71}BM$ BHJ (103c), however, with extremes shifted to the lower photon energies. Such a peculiarity can probably be a result of specific morphology, band structure of the sample with inhomogeneously distributed spin traps, as well as different energy levels occupied by spin charge carriers in the bandgap. Therefore, at the higher concentration ratio $[mF^{-\bullet}_{mob}]/[P^{+\bullet}_{loc}] \equiv [P^{+\bullet}_{mob}]/[P^{+\bullet}_{loc}]$, the better electronic properties should be expected for the respective photovoltaic system. Such a ratio obtained for the sample is also shown in the figure as function of the photon energy $h\nu_{ph}$. This parameter determined for the PCDTBT:$PC_{61}BM$ composite changes significantly with $h\nu_{ph}$ with characteristic values lying near 1.7 eV. Note that such selectivity may be used, for example, in organic optical sensors.

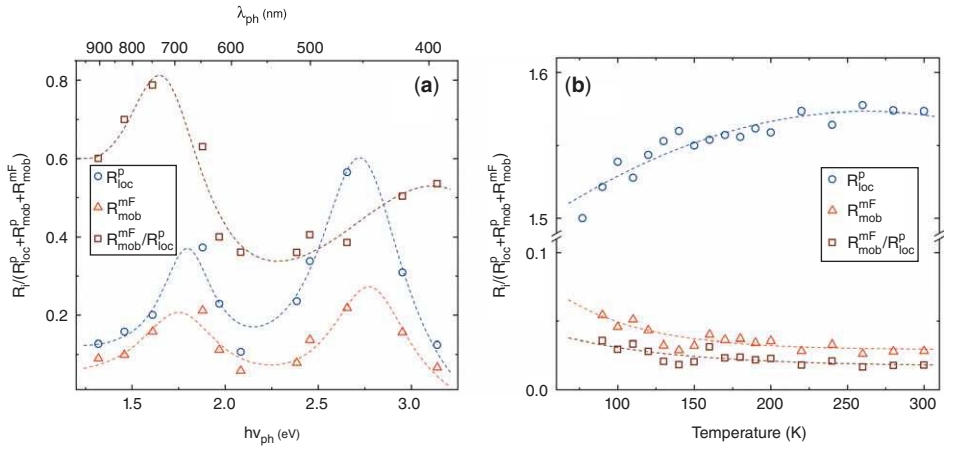

Fig. 18. Effective concentration of polarons $P^{+\bullet}_{loc}$ and methanofullerenes anion radicals $mF^{-\bullet}_{mob}$ photoinitiated in the PCDTBT:PC_{61}BM BHJ as a function of photon energy $h\nu_{ph}$ at $T = 77$ K (**a**) and of temperature under irradiation by white light with color temperature $T_c = 5500$ K (**b**). The dashed lines are drawn arbitrarily only for illustration to guide the eye.

The analysis of LEPR spectra of both the charge carriers allowed to conclude that their shape and intensity are governed not only by the number and energy of the photons absorbed but also by the temperature of BHJ. The temperature dependence of concentration of charge carriers photoinitiated in the sample by white light with color temperature $T_c = 5500$ K is shown in Figure 18**b**. The presented data may indicate a predominant effect of temperature mainly on the concentration of localized polarons. Spin susceptibility of polaron and fullerene charge carriers was determined (103a) to follow activation law with characteristic energy of 0.018 and 0.048 eV, respectively.

Peak-to-peak linewidths of polarons $P^{+\bullet}_{loc}$ and methanofullerenes anion radicals $mF^{-\bullet}_{mob}$ photoinitiated in the PCDTBT:PC_{61}BM BHJ at $T = 77$ K are shown in Figure 19 as a function of both the photon energy $h\nu_{ph}$ and temperature. It is seen from Figure 19**a** that this parameter of both charge carriers also depends on the photon energy especially at $h\nu_{ph} \approx 1.7$ eV. Such an effect can also be described in terms of the above-mentioned exchange interaction of mobile polarons with spins captured by the polymer backbone. The collision of these spins should broaden the absorption EPR line by the value determined by equation (13). Spectral linewidth of charge carriers is also feels function of temperature. Figure 19**b** demonstrates temperature dependence of these parameters obtained for these charge carriers under exposition of the composite BHJ to white light with color temperature $T_c = 5500$ K. One can note a characteristic monotonic change of these dependences with temperature. From their analysis, the activation energies of their dynamics E_a were determined from equation (13) as 0.028 and 0.013 eV, respectively (103a).

The effective spin–lattice and spin–spin relaxation times determined for all spin charge carriers from their steady-state saturated LEPR spectra are presented in Figure 20**a** as function of the photon energy $h\nu_{ph}$. Temperature

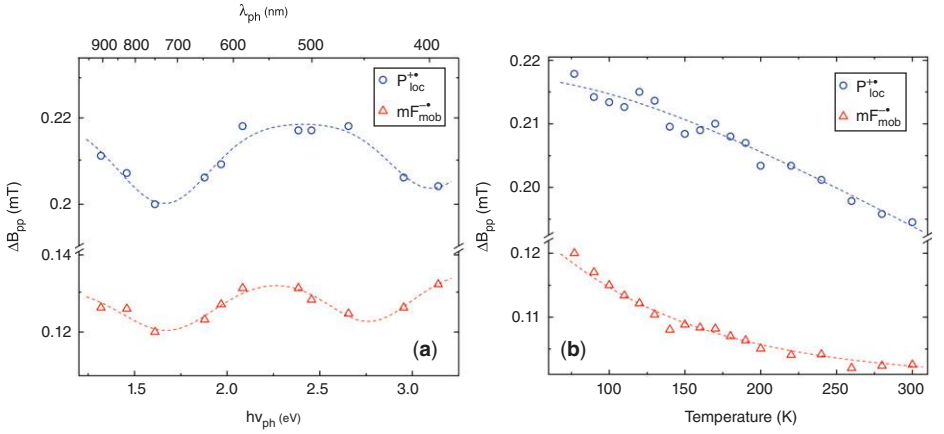

Fig. 19. The linewidth of polarons $P^{+\bullet}_{loc}$ and methanofullerenes anion radicals $mF^{-\bullet}_{mob}$ photoinitiated in the PCDTBT:$PC_{61}BM$ BHJ as a function of photon energy $h\nu_{ph}$ at $T = 77$ K (**a**) and temperature upon irradiation by white light with color temperature $T_c = 5500$ K (**b**).

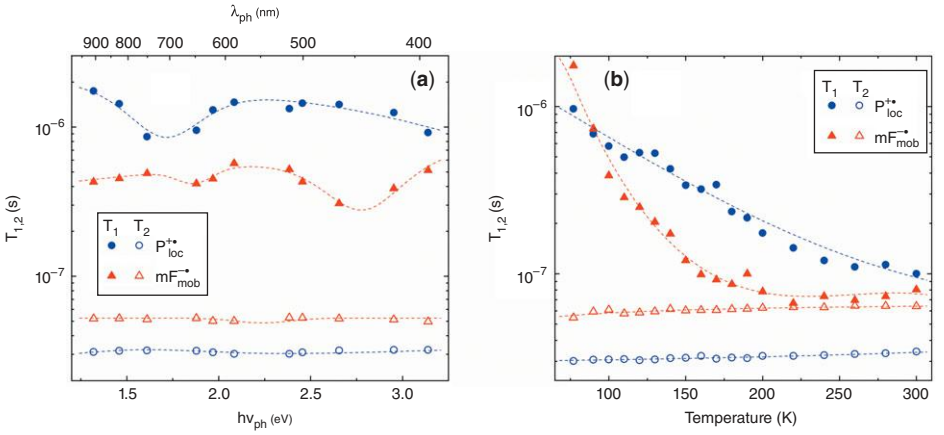

Fig. 20. Spin–lattice and spin–spin relaxation times of polarons $P^{+\bullet}_{loc}$ and methanofullerene anion radicals $mF^{-\bullet}_{mob}$ photoinitiated in the PCDTBT:$PC_{61}BM$ BHJ as a function of photon energy $h\nu_{ph}$ at $T = 77$ K (**a**) and temperature under irradiation by white light with color temperature $T_c = 5500$ K (**b**).

dependences of effective relaxation times of PC photoinitiated in the sample under its illumination by white light with the same color temperature are shown in Figure 20**b**. The data presented allow concluding selective dependence of spin–lattice relaxation time on the photon energy. This parameter of the methanofullerene radical anions is characterized by stronger temperature dependence than the polarons.

Polarons' diffusion along and between the copolymer chains with respective diffusion coefficients D_{1D} and D_{3D} as well as methanofullerene anion radicals pseudo-rotating between them with coefficients D_{rot} induces additional magnetic

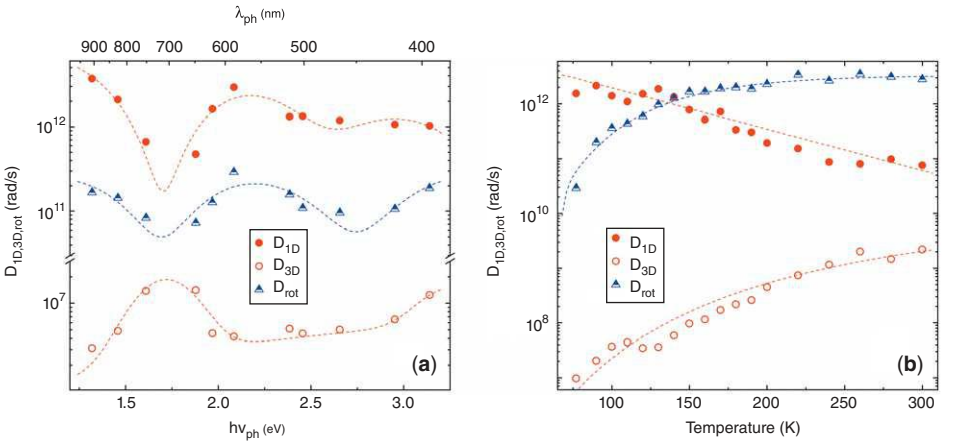

Fig. 21. Translational intrachain, D_{1D}, hopping interchain, D_{3D}, and pseudo-rotational, D_{rot}, diffusion coefficients of charge carriers photoinitiated in the PCDTBT:PC_{61}BM BHJ as a function of photon energy $h\nu_{ph}$ at $T = 77$ K (**a**) and temperature upon irradiation by white light with color temperature $T_c = 5500$ K (**b**).

fields in the copolymer matrix. This allows one to determine dynamics parameters of all PC from equations (11) and (12) with appropriate spectral density functions and the length of spin delocalization on a polaron equal to tree PCDTBT units (5d). Figure 21**a** depicts the D_{1D}, D_{3D}, and D_{rot} values as function of the photon energy $h\nu_{ph}$. It is observed from the figure that dynamic parameters of polarons in the PCDTBT:PC_{61}BM composite extremely depend on the photon energy with characteristic point lying near 1.8 eV. On the other hand, the appropriate dependence obtained for anion radicals is characterized by at least two extremes lying near 1.8 and 2.8 eV. Such peculiarity can be due to the correlation of the number and distribution of spin traps induced in the composite with the photon energy. Besides, the anisotropy of polaron dynamics D_{1D}/D_{3D} reaches a minimum at the same characteristic point that indicates the increase in dimensionality/ordering of the PCDTBT:PC_{61}BM composite. This optimizes spin dynamics and minimizes energy dispersion at charge transfer through this BHJ. Comparative analysis of the data presented shows that the deceleration of diffusion of polarons photoinitiated in the PCDTBT:PC_{61}BM BHJ narrows their contribution in the sum LEPR spectrum. This can reveal the existence of an exchange interaction between both charge carriers in the system.

The above dynamics parameters obtained for charge carriers photoinitiated in the composite BHJ under their illumination by white light with color temperature $T_c = 5500$ K are shown in Figure 21**b**.

The data obtained can be described in terms of spin scattering on the polymer lattice phonons and its thermal activation during its intrachain diffusion and interchain hopping, respectively. This allowed to determine the following spin dynamics: $E_{ph} = 0.121$ from equation (14) and $E_b = 0.079$ eV from equation (15) (103a). Pseudo-rotating mobility of the PC_{61}BM cages can be described in the framework of a semiclassical Marcus theory adopted for conjugated polymers

(106). According to this approach, methanofullerene ion radicals should reorient between copolymer layers with the rate of

$$D_{\mathrm{rot}} = D_{\mathrm{rot}}^{(0)} \frac{1}{\sqrt{4E_{\mathrm{r}}k_{\mathrm{B}}T}} \exp\left(-\frac{E_{\mathrm{r}}}{4k_{\mathrm{B}}T}\right) \tag{16}$$

where E_{r} is both the inner- and outer-sphere reorganization energy of charge carriers due to their interaction with the lattice phonons. The analysis of the experimental dependence yields $E_{\mathrm{r}} = 0.218$ eV (103a). This value is near to the required energy for activation of pure C_{60} dynamics (0.224 eV) (107); however, it exceeds the same parameter obtained for PCDTBT:PC_{71}BM BHJ (0.010 eV) (103b,c) due to a more ordered latter composite.

The results obtained show that mobile positively charged polarons and negatively charged methanofullerene anion radicals are initiated under illumination of BHJ in the PCDTBT:PC_{61}BM composite. The main part of these carriers transfers the charge, whereas some of their quantity is captured by deep spin traps reversibly initiated in the copolymer backbone. The spatial distribution, number, and energy depth of such traps depend on a structure and morphology of copolymer matrix as well as on the energy of initiating photons and the spin precession frequency.

Magnetic resonance, relaxation, and dynamics parameters of mobile and immobilized charge carriers are governed by their exchange interaction, and, therefore, all the processes carrying out in the copolymer composite become spin-assisted. Besides, these parameters were shown to be governed by the number and energy of initiating photons. The concentration of both charge carriers in the system shows extreme dependence on the photon energy with explicit extremes around 1.8 and 2.8 eV. It should be noted that the former extreme lies near the value of the energy of copolymer bandgap. Such a peculiarity can appear as a result of specific morphology and band structure of the sample with spin traps inhomogeneously distributed in its bulk and may be used in optical sensors. Anisotropic dynamics of charge carriers is also governed by the photon energy, especially when the latter value is near the bandgap of the copolymer matrix.

The sensitivity of resonant parameters to the energy of photons can be used for creation of perspective molecular electronic and spintronic elements with spin-light-field-assisted magnetic and electronic properties. Both the polarons and methanofullerene anion radicals play a role of intrachain and interlayer spin probes, respectively, taking a possibility to analyze the structure and dynamics of their environment. The methodology described can be used for the study of electronic properties of other organic multispin polymer composites.

6. Conclusion

Thus, the past years have seen extraordinary progress in synthesis and study of various macromolecular systems. EPR spectroscopy with high spectral resolution, combined with the method of spin label and probe, has helped in analyzing in detail fine structural, topological, and dynamic properties of various

macromolecular systems with paramagnetic adducts. The data obtained by multifrequency EPR method allow to correlate structural and morphological peculiarities of multispin polymer systems with their magnetic, relaxation, and electronic properties. Understanding of the fundamental factors in determining specific spin-assisted processes in such objects is now a hot topic in organic molecular science. Since coherent spin dynamics in polymers is anisotropic, our strategy seems to make it possible to obtain complex respective correlations from a multifrequency EPR study for further designing of progressive molecular electronics, spintronics, and artificial intelligence.

Acknowledgments

The author expresses his gratitude to Y. S. Lebedev, G. I. Likhtenshtein, and H.-K. Roth for collaboration and fruitful discussions.

BIBLIOGRAPHY

1. (a) J. R. C. van der Maarel, *Introduction to Biopolymer Physics*, World Scientific Publishing Co., Hackensack, N.J., 2008; (b) R. Shunmugam, ed., *Functional Polymers: Design, Synthesis, and Applications*, CRC Press, Boca Raton, Fla., 2016.
2. J. C. Glenn, T. J. Gordon, and E. Florescu, *2013-14 State of the Future*, The Millennium Project, Washington, D.C., 2014.
3. T. E. Scotheim and J. R. Reynolds, eds., *Handbook of Conducting Polymers*, vol. **3**, CRC Press, Boca Raton, Fla., 2007.
4. (a) A. J. Heeger, N. S. Sariciftci, and E. B. Namdas, *Semiconducting and Metallic Polymers*, Oxford University Press, London, 2010; (b) S. Roth and D. Carroll, *One-Dimensional Metals: Conjugated Polymers, Organic Crystals*, *Carbon Nanotubes and Graphene*, 3rd ed., Wiley-VCH Verlag GmbH & Co. KGaA, Weinheim, Germany, 2015.
5. (a) R. L. Elsenbaumer and L. W. Shacklette in T. E. Scotheim, ed., *Handbook of Conducting Polymers*, vol. **1**, Marcel Dekker, Inc., New York, 1986, pp. 213–263; (b) F. Devreux, F. Genoud, M. Nechtschein, and B. Villeret in H. Kuzmany, M. Mehring, and S. Roth, eds., *Electronic Properties of Conjugated Polymers*, vol. **76**, Springer-Verlag, Berlin, 1987, pp. 270–276; (c) M. Westerling, R. Osterbacka, and H. Stubb, *Phys. Rev. B* **66**, 165220 (2002); (d) J. Niklas, K. L. Mardis, B. P. Banks, G. M. Grooms, A. Sperlich, V. Dyakonov, S. Beaupré, M. Leclerc, T. Xu, L. Yue, and O. G. Poluektov, *Phys. Chem. Chem. Phys.* **15**, 9562–9574 (2013).
6. R. D. McCullough, S. Tristram-Nagle, S. P. Williams, R. D. Lowe, and M. Jayaraman, *J. Am. Chem. Soc.* **115**, 4910–4911 (1993).
7. M. Hultell and S. Stafstrom, *Phys. Rev. B* **75**, 104304 (2007).
8. J. L. Brédas, in T. E. Scotheim, ed., *Handbook of Conducting Polymers*, Vol. **2**, Marcel Dekker, Inc., New York, 1986, pp. 859–913.
9. J. M. Ginder and A. J. Epstein, *Phys. Rev. B* **41**, 10674–10685 (1990).
10. J. H. Bombile, M. J. Janik, and S. T. Milner, *Phys. Chem. Chem. Phys.* **18**, 12521–12533 (2018).
11. (a) T. Tanaka, *Experimental Methods in Polymer Science: Modern Methods in Polymer Research and Technology*, Academic Press, New York, 2000; (b) C. Zanardi, F. Terzi, L. Pigani, and R. Seeber, in M. Lechkov and S. Prandzheva, eds., *Encyclopedia of Polymer Composites: Properties, Performance and Applications*, Nova Science Publishers, Hauppauge, N.Y., 2009, pp. 1–74; (c) D. Rouxel, S. Thomas, and D. Ponnamma, eds., *Spectroscopy of Polymer Nanocomposites*, 1 ed., Elsevier, Oxford, UK, 2016.

12. (a) T. Kitayama and K. Hatada, *NMR Spectroscopy of Polymers*, Springer-Verlag, Berlin, 2004; (b) H. W. Spiess, in V. Percec, ed., *Hierarchical Macromolecular Structures: 60 Years after the Staudinger Nobel Prize I*, Vol. **261**, 2013, pp. 295–320.
13. E. K. Zavoisky, *J. Phys. (USSR)* **9**, 211–245 (1945).
14. (a) S. Schlick, ed., *Advanced ESR Methods in Polymer Research*, John Wiley & Sons, Inc., New York, 2006; (b) G. R. Eaton, S. S. Eaton, D. P. Barr, and R. T. Weber, *Quantitative EPR*, Springer, Vienna, Austria, 2010; (c) B. Ranby and J. F. Rabek, *ESR Spectroscopy in Polymer Research* Springer-Verlag, Berlin, 2011; (d) S. K. Misra, ed., *Multifrequency Electron Paramagnetic Resonance. Theory and Applications*, Vol. **2**, Wiley-VCH Verlag GmbH & Co. KGaA, Weinheim, Germany, 2011; (e) A. Lund, M. Shiotani, and S. Shimada, *Principles and Applications of ESR Spectroscopy*, Springer-Verlag, Germany, 2011; (f) A. Lund and M. Shiotan, eds., *EPR of Free Radicals in Solids I: Trends in Methods and Applications*, 2 ed., Vol. **1**, Springer Netherlands, Dordrecht, the Netherlands,. 2013; (g) A. Lund and M. Shiotan, eds., *EPR of Free Radicals in Solids II: Progress in Theoretical Chemistry and Physics*, 2 ed., vol. **2**, Springer Netherlands, 2013; (h) P. G. Baranov, H. J. von Bardeleben, F. Jelezko, and J. Wrachtrup, *Magnetic Resonance of Semiconductors and Semiconductor Nanostructures*, Springer-Verlag, Vienna, Austria, 2017; (i) D. Goldfarb and S. Stoll, eds., *EPR Spectroscopy: Fundamentals and Methods*, Wiley-VCH Verlag GmbH & Co. KGaA, Weinheim, Germany, 2018; (j) C. Karunakaran, *Spin Resonance Spectroscopy: Principles and Applications* 1 ed., Elsevier, Amsterdam, the Netherlands, 2018; (k) D. Goldfarb and S. Stoll, eds., *EPR Spectroscopy: Fundamentals and Methods*, John Wiley & Sons, Inc., Hoboken, N.J., 2018.
15. K-u-R. Naveed, L. Wang, H. Yu, R. S. Ullah, M. Haroon, S. Fahad, J. Li, T. Elshaarani, R. U. Khan, and A. Nazir, *Polym. Chem.* **9**, 3306–3335 (2018).
16. A. L. Buchachenko, C. N. Turton, and T. I. Turton, *Stable Radicals*, Consultants Bureau, New York, 1995.
17. S. A. Altshuler and B. M. Kozirev, *Electron Paramagnetic Resonance*, Academic Press, New York, 1972.
18. (a) W. B. Mims, in S. Geschwind, ed., *Electron Paramagnetic Resonance*, Plenum Press, New York, 1972, pp. 263–351; (b) K. M. Salikhov, A. G. Semenov, and Y. D. Tsvetkov, *Electron Spin Echo and its Utilization*, Nauka, Novosibirsk, USSR, 1976 (in Russian).
19. S. Geschwind, in S. Geschwind, ed., *Electron Paramagnetic Resonance*, Plenum Press, New York, 1972, Ch. 5, pp. 353–425.
20. (a) C. P. Poole, *Electron Spine Resonance*, International Science Publishers, London, 1967; (b) L. Kevan and L. D. Kispert, *Electron Spin Double Resonance Spectroscopy*, Wiley Interscience, New York, 1976.
21. (a) A. M. Wasserman and T. N. Khazanovich, in R. A. Pathrick, ed., *Polymer Yearbook*, Vol. **12**, Taylor & Francis, London, 1995, pp. 153–184; (b) L. Berliner and J. Reuben, eds., *Spin Labeling: Theory and Applications*, Vol. **8**, Springer Science & Business Media, New York, 2012; (c) C. R. Timmel and J. R. Harmer, eds., *Structural Information from Spin-Labels and Intrinsic Paramagnetic Centres in the Biosciences*, Springer-Verlag, Berlin, Germany, 2013.
22. (a) J. S. Hyde and L. R. Dalton, in L. J. Berliner, ed., *Spin Labeling II: Theory and Application*, Vol. **2**, Academic Press, New York, 1979, Ch. 1, pp. 1–70; (b) S. S. Eaton, G. R. Eaton, and L. J. Berliner, eds., *Biomedical EPR—Part B: Methodology, Instrumentation, and Dynamics*, Springer, New York, 2005.
23. (a) O. Y. Grinberg, A. A. Dubinskii, V. F. Shuvalov, L. G. Oransky, V. I. Kurochkin, and Y. S. Lebedev, *Dokl. Acad. Sci. USSR* **230**, 884–886 (1976); (b) O. Y. Grinberg, A. A. Dubinskii, and Y. S. Lebedev, *Russ. Chem. Rev*. **52**, 1490–1513 (1983); (c) V. I. Krinichnyi, *J. Biochem. Biophys. Methods* **23**, 1–30 (1991); (d) V. I. Krinichnyi, *Appl. Magn. Reson*. **2**, 29–60 (1991); (e) V. I. Krinichnyi, *2-mm Wave Band EPR Spectroscopy of Condensed*

Systems, CRC Press, Boca Raton, Fla., 1995; (f) O. Y. Grinberg and L. J. Berliner, eds., *Very High Frequency (VHF) ESR/EPR*, Vol. **22**, Kluwer Academic/Plenum Publishers, New York, 2004; (g) V. I. Krinichnyi, in S. Schlick, ed., *Advanced ESR Methods in Polymer Research*, John Wiley & Sons., inc., Hoboken, NJ, 2006, Ch. 12, pp. 307–338; (h) V. I. Krinichnyi, *2-mm Wave Band EPR Spectroscopy of Condensed Systems*, CRC Press Taylor & Francis Group, Boca Raton, Fla., 2017.

24. V. I. Krinichnyi, A. E. Pelekh, Y. S. Lebedev, L. I. Tkachenko, G. I. Kozub, A. L. Barra, L. C. Brunel, and J. B. Robert, *Appl. Magn. Reson.* **7**, 459–467 (1994).
25. (a) Y. S. Lebedev in N. M. Atherton, M. J. Davies, and B. C. Gilbert, eds., *Electron Spin Resonance*, vol. **14**, Royal Society of Chemistry, Cambridge, UK, 1994, pp. 63–87; (b) S. S. Eaton and G. R. Eaton, in C. P. Poole and H. A. Farach, eds., *Handbook of Electron Spin Resonance*, Vol. **2**, Springer-Verlag, New York, 1999, pp. 344–367; (c) W. R. Hagen, *Coord. Chem. Rev.* **192**, 209–229 (1999); (d) G. M. Smith and P. C. Riedi, *Progress in High Field EPR*, RSC, Cambridge, UK, 2000; (e) D. Marsh, D. Kurad, and V. A. Livshits, *Chem. Phys. Lipids* **116**, 93–114 (2002); (f) E. J. Hustedt and A. H. Beth, *Biophys. J*. **86**, 3940–3950 (2004); (g) V. I. Krinichnyi, in M. Lechkov and S. Prandzheva, eds., *Encyclopedia of Polymer Composites: Properties, Performance and Applications*, Nova Science Publishers, Hauppauge, N.Y., 2009, Ch. 11, pp. 417–446; (h) O. Grinberg and L. Berliner, eds., *Very High Frequency (VHF) ESR/EPR (Biological Magnetic Resonance)*, Springer-Verlag, New York, 2011; (i) V. I. Krinichnyi, in M. C. Wythers, ed., *Advances in Materials Science Research*, Vol. **17**, Nova Science Publishers, Hauppauge, N.Y., 2014, Ch. 5, pp. 109–160; (j) V. I. Krinichnyi, in S. Thomas, D. Rouxel, and D. Ponnamma, eds., *Spectroscopy of Polymer Nanocomposites*, 1 ed., Elsevier, Amsterdam, the Netherlands, 2016, Ch. 9, pp. 202–275; (k) V. I. Krinichnyi, *Multi Frequency EPR Spectroscopy of Conjugated Polymers and Their Nanocomposites*, CRC Press Taylor & Francis Group, Boca Raton, Fla., 2016; (l) V. I. Krinichnyi, in A. Laref, ed., *Polarons: Recent Progress and Perspectives*, Nova Science Publishers, Inc., Hauppauge, N.Y., 2018, Ch. 1.
26. (a) M. R. Brustolon and E. Giamello, eds., *Electron Paramagnetic Resonance Spectroscopy: A Practitioner's Toolkit*, John Wiley & Sons, Inc., 2009; (b) L. Que, ed., *Physical Methods in Bioinorganic Chemistry, Spectroscopy and Magnetism*, University Science Books, Sausalito, Calif. 2010; (c) A. Lund and M. Shiotani, eds., *Applications of EPR in Radiation Research*, Springer-Verlag, Berlin, Germany 2014.
27. C. P. Poole, *Electron Spin Resonance, A Comprehensive Treatise on Experimental Techniques*, John Wiley & Sons, Inc., New York, 1983.
28. F. Herlach, ed., *Strong and Ultrastrong Magnetic Fields and Their Applications*, Vol. **67**, Springer-Verlag, Berlin, Germany, 1985.
29. K. Mizoguchi and S. Kuroda, in H. S. Nalwa, ed., *Handbook of Organic Conductive Molecules and Polymers*, Vol. **3**, John Wiley & Sons, Ltd., Chichester, UK, 1997, Ch. 6, pp. 251–317.
30. J. H. Freed, in A. Ohta, A. Kawamori, and J. Yamauchi, eds., *EPR in the 21st Century*, Elsevier Science, Amsterdam, the Netherlands, 2002, pp. 719–730.
31. (a) W. Weltner, *Magnetic Atoms and Molecules*, Scientific and Academic Editions, New York, 1983; (b) A. Potapov and D. Goldfarb, *Appl. Magn. Reson.* **37**, 845–850 (2010); (c) R. Kaufmann, I. Yadid, and D. Goldfarb, *J. Magn. Reson*. **230**, 220–226 (2013).
32. H. A. Kuska and M. T. Rogers in E. T. Kaiser and L. Kevan, eds., *Radical Ions*, John Wiley & Sons, New York, 1968, pp. 579–745.
33. V. I. Krinichnyi, E. I. Yudanova, and B. Wessling, *Synth. Met.* **179**, 67–73 (2013).
34. S. V. Kolaczkowski, J. T. Cardin, and D. E. Budil, *Appl. Magn. Reson.* **16**, 293–298 (1999).
35. V. I. Krinichnyi, Y. S. Lebedev, and O. Y. Grinberg, *Appl. Magn. Reson.* **13**, 259–267 (1997).

36. A. E. Pelekh, V. I. Krinichnyi, A. Y. Brezgunov, L. I. Tkachenko, and G. I. Kozub, *Polym. Sci.* **33**, 1615–1623 (1991).
37. S. B. Orlinski, J. Schmidt, E. N. Mokhov, and P. G. Baranov, *Phys. Rev. B* **67**, 125207 (2003).
38. P. R. Surján, *Int. J. Quantum Chem* **63**, 425–435 (1997).
39. W. Harneit, *Phys. Rev. A* **65**, 032322 (2002).
40. A. Stesmans and G. van Gorp, *Rev. Sci. Instrum.* **60**, 2949–2952 (1989).
41. R. A. Wind, S. Bai, J. Z. Hu, M. S. Solum, P. D. Ellis, D. M. Grant, R. J. Pugmire, C. M. V. Taylor, and C. R. Yonker, *J. Magn. Reson.* **143**, 233–239 (2000).
42. (a) V. I. Krinichnyi, A. E. Pelekh, H. K. Roth, and K. Lüders, *Appl. Magn. Reson*. **4**, 345–356 (1993); (b) V. I. Krinichnyi, N. N. Denisov, H. K. Roth, E. Fanghänel, and K. Lüders, *Polym. Sci. A* **40**, 1259–1269 (1998); (c) V. I. Krinichnyi, *Synth. Met*. **108**, 173–222 (2000); (d) V. I. Krinichnyi, H. K. Roth, and M. Schrödner, *Appl. Magn. Reson*. **23**, 1–17 (2002).
43. A. E. Pelekh, L. M. Goldenberg, and V. I. Krinichnyi, *Synth. Met.* **44**, 205–211 (1991).
44. A. A. Dubinski, O. Y. Grinberg, V. I. Kurochkin, L. G. Oransky, O. G. Poluektov, and Y. S. Lebedev, *Theor. Exp. Chem.* **17**, 231–236 (1981).
45. O. Y. Grinberg, A. A. Dubinski, O. G. Poluektov, and Y. S. Lebedev, *Theor. Exp. Chem.* **17**, 806–813 (1981).
46. L. M. Goldenberg and V. I. Krinichnyi, *Synth. Met.* **53**, 403–407 (1993).
47. P. Bernier, in T. E. Scotheim, ed., *Handbook of Conducting Polymers*, vol. **2**, Marcel Dekker Inc., New York, 1986, pp. 1099–1125.
48. A. S. Davydov, *Solitons in Molecular Systems*, Springer-Science & Business Media, B.V., Dordrecht, the Netherlands 1985.
49. L. Brizhik, A. Eremko, B. Piette, and W. Zakrzewski, *Int. J. Quantum Chem.* **110**, 25–37 (2010).
50. G. I. Likhtenstein, *Spin-Labeling Methods in Molecular Biology*, Wiley Interscience, New York, 1989.
51. (a) A. Marek, M. A. Voinov, and A. I. Smirnov, *Cell Biochem Biophys*. **75**, 211–226 (2017); (b) S. A. Dzuba, M. N. Uvarov, D. E. Utkin, F. Formaggio, A. Bedon, A. Orlandin, and C. Peggion, *Appl. Magn. Reson.* **48**, 943–953 (2017).
52. (a) V. I. Krinichnyi, O. Y. Grinberg, I. K. Yusupov, R. M. Marupov, P. K. Bobodzhanov, G. I. Likhtenstein, and Y. S. Lebedev, *Biofizika* **31**, 482–485 (1986); (b) V. I. Krinichnyi, E. N. Ushakov, K. A. Arutyunyan, and N. V. Kostina, *Biofizika* **36**, 427–431 (1991).
53. E. V. Lyubashevskaya, L. I. Antsiferova, and Y. S. Lebedev, *Theor. Exp. Chem.* **23**, 46–53 (1987).
54. M. E. Johnson, *Biochemistry* **17**, 1223–1228 (1978).
55. B. G. Ershov and A. S. Klimentov, *Russ. Chem. Rev.* **53**, 1195–1207 (1984).
56. A. Jayaraman, inG. D. Considine ed., *Van Nostrand's Encyclopedia of Chemistry*, John Wiley & Sons, Hoboken, N.J., 2005, pp. 1–10.
57. (a) J. Rodriguez, H. J. Grande, and T. F. Otero in H. S. Nalwa, ed., *Handbook of Organic Conductive Molecules and Polymers*, Vol. **2**, John Wiley & Sons., Ltd, Chichester, 1997, pp. 415–468; (b) J. Janata and M. Josowicz, *Nat. Mater*. **2**, 19–24 (2003).
58. A. J. Epstein, in J. E. Mark, ed., *Physical Properties of Polymers. Handbook*, 2 ed., Springer-Verlag, Berlin, Germany, 2007, Ch. 46, pp. 725–744.
59. B. R. Saunders, R. J. Fleming, and K. S. Murray, *Chem. Mater.* **7**, 1082–1094 (1995).
60. M. Taunk and S. Chand in V. K. Jain and A. Verma, eds., *Physics of Semiconductor Devices*, Springer, Heidelberg, Germany, 2014, pp. 903–904.
61. H. Sakamoto, N. Kachi, K. Mizoguchi, K. Yoshioka, S. Masubuchi, and S. Kazama, *Synth. Met.* **101**, 481–481 (1999).
62. K. Kanemoto and J. Yamauchi, *J. Phys. Chem. B* **105**, 2117–2121 (2001).

63. (a) K. Kanemoto and J. Yamauchi, *Synth. Met.* **114**, 79–84 (2000); (b) K. Kanemoto and J. Yamauchi, *Phys. Rev. B* **61**, 1075–1082 (2000).
64. (a) J. C. Scott, P. Pfluger, M. T. Kroumbi, and G. B. Street, *Phys. Rev. B* **28**, 2140–2145 (1983); (b) S. Chakrabarti, B. Das, P. Banerji, D. Banerjee, and R. Bhattacharya, *Phys. Rev. B* **60**, 7691–7694 (1999).
65. H. Winter, G. Sachs, E. Dormann, R. Cosmo, and H. Naarmann, *Synth. Met.* **36**, 353–365 (1990).
66. A. L. Buchachenko, *Complexes of Radicals and Molecular Oxygen with Organic Molecules (Russ)*, Nauka, Moscow, USSR, 1984.
67. A. Reddoch and S. Konishi, *J. Chem. Phys.* **70**, 2121 (1979).
68. A. L. Buchachenko and A. M. Vasserman, *Stable Radicals (Russ)*, Khimija, Moscow, USSR, 1973.
69. J. M. Williams, J. R. Ferraro, R. J. Thorn, K. D. Carlson, U. Geiser, H. H. Wang, A. M. Kini, and M. H. Whangboo, *Organic Superconductors (Including Fullerenes): Synthesis, Structure, Properties, and Theory*, Prentice-Hall, Inc., Englewood Cliffs, N.J., 1992.
70. F. Faridbod, M. R. Ganjali, R. Dinarvand, and P. Norouzi, *Sensors* **8**, 2331–2412 (2008).
71. H. K. Roth, H. Gruber, E. Fanghänel, and T. V. Quang, *Prog. Colloid Polym. Sci.* **78**, 75–78 (1988).
72. H. Gruber, H. K. Roth, J. Patzsch, and E. Fanghänel, *Makromolek. Chem.-Macromolec. Symp.* **37**, 99–113 (1990).
73. (a) H. K. Roth, H. Gruber, G. Voelkel, W. Brunner, and E. Fanghänel, *Prog. Colloid Polym. Sci*. **80**, 254–263 (1989); (b) H. K. Roth, W. Brunner, G. Volkel, M. Schrödner, and H. Gruber, *Makromolek. Chem.-Macromolec. Symp*. **34**, 293–307 (1990); (c) J. Patzsch and H. Gruber, in H. Kuzmany, M. Mehring, and S. Roth, eds., *Electronic Properties of Polymers*, Vol. **107**, Springer-Verlag, Berlin, Germany, 1992, pp. 121–124.
74. V. I. Krinichnyi, O. Y. Grinberg, I. B. Nazarova, G. I. Kozub, L. I. Tkachenko, M. L. Khidekel, and Y. S. Lebedev, *Bull. Acad. Sci. USSR, Chem. Div.* **34**, 425–427 (1985).
75. P. R. Cullis, *J. Magn. Reson.* **21**, 397–418 (1976).
76. V. I. Krinichnyi, A. E. Pelekh, A. Y. Brezgunov, L. I. Tkachenko, and G. I. Kozub, *Mater. Sci. Eng.* **17**, 25–29 (1991).
77. (a) F. Carrington and A. D. McLachlan, *Introduction to Magnetic Resonance with Application to Chemistry and Chemical Physics*, Harrer & Row, Publishers, New York, 1967; (b) A. Abragam, *Principles of Nuclear Magnetism*, Clarendon Press, Oxford, UK, 1983.
78. F. Devreux and H. Lecavelier, *Phys. Rev. Lett.* **59**, 2585–2587 (1987).
79. Z. H. Wang, E. M. Scherr, A. G. MacDiarmid, and A. J. Epstein, *Phys. Rev. B* **45**, 4190–4202 (1992).
80. A. Madhukar and W. Post, *Phys. Rev. Lett.* **39**, 1424–1427 (1977).
81. (a) E. A. Silinsh, *Organic Molecular Crystals: Their Electronic States*, Springer-Verlag, Berlin, Germany, 1980; (b) E. Silinsh, *Organic Molecular Crystals: Interaction, Localization, and Transport Phenomena*, American Institute of Physics, New York, 1994.
82. (a) S. S. Sun and N. S. Sariciftci, eds., *Organic Photovoltaics: Mechanisms, Materials, and Devices (Optical Engineering)*, CRC Press, Boca Raton, Fla., 2005; (b) J. Poortmans and V. Arkhipov, eds., *Thin Film Solar Cells: Fabrication, Characterization and Applications* John Wiley & Sons, Ltd., West Sussex, UK, 2006; (c) M. Jeffries-El and R. D. McCullough, in T. E. Scotheim and J. R. Reynolds, eds., *Handbook of Conducting Polymers*, Vol. **3d**, CRC Press, Boca Raton, Fla., 2007, Ch. 9, pp. 9-1 to 9-49; (d) M. Pagliaro, G. Palmisano, and R. Ciriminna, *Flexible Solar Cells*, Wiley-VCH Verlag GmbH & Co. KGaA, Weinheim, Germany, 2008; (e) C. Brabec, U. Scherf, and V. Dyakonov, eds., *Organic Photovoltaics: Materials, Device Physics, and Manufacturing Technologies*, 2 ed., Vol. **1**, Wiley-VCH Verlag GmbH & Co. KGaA, Weinheim, Ger-

many, 2014; (f) J. Zaumseil, in S. Ludwigs, ed., *P3HT Revisited: From Molecular Scale to Solar Cell Devices*, vol. **265**, 2014, pp. 107–137.
83. R. D. McCullough, R. D. Lowe, M. Jayaraman, P. C. Ewbank, and D. L. Anderson, *Synth. Met.* **55**, 1198–1203 (1993).
84. (a) E. M. Conwell ,in H. S. Nalwa, ed., *Handbook of Organic Conductive Molecules and Polymers*, Vol. **4**, John Wiley & Sons, Ltd., Chichester, UK, 1997, pp. 1–45; (b) R. Menon in H. S. Nalwa, ed., *Handbook of Organic Conductive Molecules and Polymers*, Vol. **4**, John Wiley & Sons, Ltd., Chichester, UK, 1997, pp. 47–145.
85. J. Bobacka, A. Ivaska, and A. Lewenstam, *Anal. Chim. Acta* **385**, 195–202 (1999).
86. (a) N. S. Sariciftci and A. J. Heeger, *Synth. Met*. **70**, 1349–1352 (1995); (b) D. Gebeyehu, F. Padinger, T. Fromherz, J. C. Hummelen, and N. S. Sariciftci, *Bull. Chem. Soc. Ethiopia* **14**, 57–68 (2000); (c) D. Gebeyehu, C. J. Brabec, F. Padinger, T. Fromherz, J. C. Hummelen, D. Badt, H. Schindler, and N. S. Sariciftci, *Synth. Met*. **118**, 1–9 (2001).
87. T. Kaniowski, S. Niziol, J. Sanetra, M. Trznadel, and A. Proń, *Synth. Met.* **94**, 111–114 (1998).
88. (a) H. K. Roth and V. I. Krinichnyi, *Synth. Met*. **137**, 1431–1432 (2003); (b) V. I. Krinichnyi and H. K. Roth, *Appl. Magn. Reson*. **26**, 395–415 (2004).
89. V. I. Krinichnyi, *Russ. Chem. Rev.* **65**, 521–536 (1996).
90. (a) Y. N. Molin, K. M. Salikhov, and K. I. Zamaraev, *Spin Exchange*, Springer-Verlag, Berlin, Germany, 1980; (b) E. Houze and M. Nechtschein, *Phys. Rev. B* **53**, 14309–14318 (1996).
91. (a) M. A. Butler, L. R. Walker, and Z. G. Soos, *J. Chem. Phys*. **64**, 3592–3601 (1976); (b) M. Nechtschein, in T. A. Skotheim, R. L. Elsenbaumer, and J. R. Reynolds, eds., *Handbook of Conducting Polymers*, Marcel Dekker, Inc., New York, 1997, pp. 141–163.
92. Y. Kunugi, Y. Harima, K. Yamashita, N. Ohta, and S. Ito, *J. Mater. Chem.* **10**, 2673–2677 (2000).
93. S. Masubuchi, R. Imai, K. Yamazaki, S. Kazama, J. Takada, and T. Matsuyama, *Synth. Met.* **101**, 594–595 (1999).
94. S. Kivelson and A. J. Heeger, *Synth. Met.* **22**, 371–384 (1988).
95. F. Huang, H.-L. Yip, and Y. Cao, eds., *Polymer Photovoltaics: Materials, Physics, and Device Engineering*, The Royal Society of Chemistry, Cambridge, UK, 2015.
96. J. M. Lupton, D. R. McCamey, and C. Boehme, *Chem. Phys. Chem.* **11**, 3040–3058 (2010).
97. O. A. Ibraikulov, C. Ngov, P. Chavez, I. Bulut, B. Heinrich, O. Boyron, K. L. Gerasimov, D. A. Ivanov, S. Swaraj, S. Mery, N. Leclerc, P. Leveque, and T. Heiser, *J. Mater. Chem. A* **6**, 12038–12045 (2018).
98. (a) M. Liedtke, A. Sperlich, H. Kraus, A. Baumann, C. Deibel, M. J. M. Wirix, J. Loos, C. M. Cardona, and V. Dyakonov, *J. Am. Chem. Soc*. **133**, 9088–9094 (2011); (b) V. I. Krinichnyi, *Sol. Energy Mater. Sol. Cells* **92**, 942–948 (2008); (c) V. I. Krinichnyi and E. I. Yudanova, *Sol. Energy Mater. Sol. Cells* **95**, 2302–2313 (2011); (d) J. Niklas and O. G. Poluektov, *Adv. Energy Mater*. **7**, 1602226 (2017).
99. (a) G. Li, R. Zhu, and Y. Yang, *Nat. Photonics* **6**, 153–161 (2012); (b) L. Kaake, D. Moses, C. Luo, A. K. K. Kyaw, L. A. Perez, S. Patel, M. Wang, B. Grimm, Y. Sun, G. C. Bazan, E. J. Kramer, and A. J. Heeger, in F. Huang, H.-L. Yip, and Y. Cao, eds., *Polymer Photovoltaics: Materials, Physics, and Device Engineering*, 2015, Ch. 8, pp. 255–271.
100. (a) X. H. Lu, H. Hlaing, D. S. Germack, J. Peet, W. H. Jo, D. Andrienko, K. Kremer, and B. M. Ocko, *Nat. Commun*. **3**, 1290/01 - 1290/07 (2012); (b) J. S. Moon, J. Jo, and A. J. Heeger, *Adv. Energy Mater.* **2**, 304–308 (2012).
101. (a) N. Berton, C. Ottone, V. Labet, R. de Bettignies, S. Bailly, A. Grand, C. Morell, S. Sadki, and F. Chandezon, *Macromol. Chem. Phys*. **212**, 2127–2141 (2011); (b) J. Kim, M. H. Yun, G. H. Kim, J. Y. Kim, and C. Yang, *Polym. Chem*. **3**, 3276–3281 (2012).

102. O. G. Poluektov, S. Filippone, N. Martín, A. Sperlich, C. Deibel, and V. Dyakonov, *J. Phys. Chem. B* **114**, 14426–14429 (2010).
103. (a) V. I. Krinichnyi, E. I. Yudanova, and N. N. Denisov, *J. Chem. Phys*. **141**, 044906 (2014); (b) V. I. Krinichnyi and E. I. Yudanova, *Synth. Met.* **210**, 148–155 (2015); (c) V. I. Krinichnyi and E. I. Yudanova, *IEEE J. Photovolt*. **6**, 506–515 (2016); (d) V. I. Krinichnyi, E. I. Yudanova, and V. R. Bogatyrenko, *J. Phys. Chem. Solids* **111**, 153–159 (2017); (e) V. I. Krinichnyi, E. I. Yudanova, and V. R. Bogatyrenko, *Sol. Energy Mater. Sol. Cells* **174**, 333–341 (2018).
104. M. Tachiya and K. Seki, *Phys. Rev. B* **82**, 085201 (2010).
105. J. Kočka, S. R. Elliott, and E. A. Davis, *J. Phys. C: Solid State Phys.* **12**, 2589–2596 (1979).
106. (a) A. Van Vooren, J.-S. Kim, and J. Cornil, *Chem. Phys. Chem.* **9**, 989–993 (2008); (b) Y.-K. Lan and C.-I. Huang, *J. Phys. Chem. B* **112**, 14857–14862 (2008).
107. B. Morosin, Z. B. Hu, J. D. Jorgensen, S. Short, J. E. Schirber, and G. H. Kwei, *Phys. Rev. B* **59**, 6051–6057 (1999).

Glossary

A_{ii}	Principal values of the hyperfine tensor
a_{iso}	Isotropic huperfine interaction constant, mT
B	Magnetic field, 1 $T = 10^4$ Oe, G
B_0	External magnetic field modulus
B_1	Amplitude of magnetic term of MW polarizing field
$D_{\mathrm{1D,3D}}$	Intra- and interchain diffusion coefficients, respectively, rad/s
D_{rot}	Rotational diffusion coefficient, rad/s
E	Energy, 1 eV = $1.60217733 \times 10^{-19}$, $J = 8.06557982 \times 10^3$ cm^{-1} = 2.41800×10^{14} Hz
E_{a}	Activation energy
E_{b}	Spin barrier crossing energy
E_{ph}	Energy of lattice phonons
E_{r}	Charge carrier reorganization energy, eV
g	Landé splitting factor, $g_{\mathrm{e}} = 2.00231930436153_{53}$ for free electron
g_{ii}	Principal values of the splitting tensor
g_{iso}	Isotropic (averaged) g-factor equal to $1/3(g_{\mathrm{xx}} + g_{\mathrm{yy}} + g_{\mathrm{zz}})$ or $1/3(2g_{\perp} + g_{\parallel})$
$g(\omega)$	Factor of line shape
$h = 2\pi\hbar$	Planck quantum constant, $h = 6.6260755 \times 10^{-34}$ J s
I	Total nuclear spin of molecule
$J(\omega)$	Spectral density function
k_{B}	Boltzmann constant, $k_{\mathrm{B}} = 1.380658 \times 10^{-23}$ J K^{-1}
k_{f}	Filling coefficient
N	Spin number
n	Spin/charge concentration per a monomer unit
p_{ff}	Probability of spin flip-flop
Q_0	Unloaded quality factor of spectrometer cavity
r_{NO}	Distance between N and O atoms in the nitroxide radical
S	Total electron spin of molecule
t	Charge transfer integral, eV
t	Time, s

T_1	Electron longitudinal (spin–lattice) relaxation time
T_{1p}	Proton longitudinal (spin–lattice) relaxation time
T_2	Electron transverse (spin–spin) relaxation time
T_c	Characteristic temperature
t_{cc}	Resonant overlapping integral of C=C bond
T_g	Matrix glass transition temperature
$U(\omega t)$	Dispersion signal term
V	Sample volume
	$g(\omega)\sin(\omega t - \varphi)$ in-phase (φ=0), out-of-phase (φ=$-\pi$), and π/2-out-of-phase (φ=$\pm\pi/2$) (in phase quadrature) dispersion signal terms registered at φ shift in a phase detector with respect to applied modulation
u_i	Amplitude of ith dispersion signal
v_F	Velocity of spin diffusion near the Fermi level, cm/s
x, y, z	Axes of molecular coordinate system
y	Doping level
γ_e	Hyromagnetic ratio for electron, $\gamma_e = 1.760859708_{39} \times 10^{11}$ T^{-1} s^{-1}
Δ	Half-bandgap.
ΔB_{pp}	Linewidth from peak to peak
$\langle \Delta\omega^2 \rangle$	Averaged constant of dipole spin interaction in a powder sample
δ	Gamma function
$\delta(\Delta\omega)$	Spectral line broadening
ε	Dielectric constant
ε_0	Dielectric constant for vacuum
η	Coefficient of dynamic viscosity
θ	Torsion (dihedral) angle
λ	Spin–orbit coupling constant, eV
μ	Dipole moment of spin-modified molecule
μ_0	Permeability for vacuum, $\mu_0 = 4\pi \times 10^{-7}$ V s A^{-1} m^{-1}
μ_B	Bohr magneton, $\mu_B = 9.27400968_{20} \times 10^{-24}$ J T^{-1}
μ_u	Dipole moment of spin probe
$\rho(0)$	Spin density on lattice unit
ν_e	Resonance frequency of free electron precession, $\nu_e = \omega_e/\pi$
ν_l	Libration frequency, s^{-1}
ν_{ph}	Photon frequency
Σ_{ij}	Lattice sum for powder
σ	Intrinsic conductivity
σ_{ac}	Alternating current electric conductivity, S/m
σ_{dc}	Direct current electric conductivity, S/m
τ	Effective relaxation time
τ_c	Correlation time of radical rotation
τ_m	Mechanical relaxation time
φ	Spin macroprobe orientation angle
χ	Static magnetic susceptibility of spin ensemble
χ'	Dispersion real term of magnetic susceptibility
χ''	Absorption imaginary term of magnetic susceptibility.
ω_e	Angular resonance frequency of electron transition between α and β levels

ω_{hop}	Angular frequency of spin-hopping diffusion
ω_l	Angular libration frequency, rad/s
ω_m	Angular frequency of Zeeman magnetic modulation, rad/s

Abbreviations and Acronyms

ac	alternating current
BHJ	bulk heterojunctions
CB	conducting band
CW	continuous wave
$(DBTTF)_3PtBr_6$	$(dibenzotetrathiafulvalene)_3PtBr_6$
dc	direct current
DPPH	2,2-Diphenyl-1-picrylhydrazyl
ENDOR	Electron nuclear double resonance
EPR	Electron paramagnetic resonance
LEPR	Light-induced electron paramagnetic resonance
MW	Microwave (frequency)
NMR	Nuclear magnetic resonance
P3AT	Poly(3-alkylthophene)
P3DDT	Poly(3-dodecylthophene)
P3HT	Poly(3-hexylthophene)
P3OT	Poly(3-octylthophene)
PANI	Polyaniline
PANI-EB	Emeraldine base form of polyaniline
PC	Paramagnetic centers
$PC_{x1}BM$	[6,6]-phenyl-C_{x1}-butanoic acid methyl ester
PCDTBT	Poly[N-9′-hepta-decanyl-2,7-carbazole-alt-5,5-(4′,7′-di-2-thienyl-2′,1′,3′-benzothiadiazole)]
PPP	Poly(*p*-phenylene)
PT	Polythiophene
PTFE	Poly(1,1,2,2-tetrafluoroethylene)
PTTF	Polytetrathiafulvalene
PVC	Polyvinyl chloride
QxD	Quasi-x-dimensionality
RT	Room temperature
ST-EPR	Saturation transfer Electron Paramagnetic Resonance
Trans-PA	*trans*-Polyacetylene
TTF	Tetrathiafulvalene
VB	Valence band
VRH	Variable range hopping

VICTOR I. KRINICHNYI
Department of Kinetics and Catalysis,
Institute of Problems of Chemical Physics
Chernogolovka, Moscow Region,
Russian Federation